Elementary Reaction-based Kinetic Model for the Fate of *N*-nitrosodimethylamine in UV Oxidation

Supporting Information

Content:

Benjamin Barrios[1], Divya Kamath[1], Erica Coscarelli[1], and Daisuke Minakata[1*]

[1]Department of Civil and Environmental Engineering, Michigan Technological University

*Corresponding author. Phone: +1-906-487-1830; Fax: +1-906-487-2943, 1400 Townsend Drive, Houghton MI, 49931, U.S.

Email address: dminakat@mtu.edu

Text S1: Aqueous-phase Computational Calculations

The structures of molecules and radicals in their ground state were determined using the Berny geometry optimization algorithm[1] using GEDIIS[2] in redundant internal coordinate. The structure at transition states were searched as first-order saddle points on the potential energy surface using the quadratic synchronous transit method (QST)[3,4]. The transition state was verified by a single negative frequency, which indicated the saddle point. We did not include anharmonicity from hindered rotors and basis set superposition errors (BSSE) due to their minor contribution.[5] The tunneling effect was accounted and included in the free energy calculation using Wigner's equation: -RTlnγ(T), where R is the gas constant, T is the absolute temperature, and γ(T) is the transmission coefficient that represents the effect of tunneling at temperature T.[6,7] The free energy changes associated with moving from a gaseous phase at 1 atm to an aqueous concentration was included in the calculation of free energies of solvation calculated by the SMD solvation method.[8]

The theoretically calculated aqueous-phase free energy of activation, $\Delta G^{\text{act}}_{\text{aq,calc}}$, is defined as a quasi-thermodynamic molar free energy of activation at a given temperature T[7] and can be calculated by

$$\Delta G^{\text{act}}_{\text{aq,calc}} = \Delta G^{\text{TS}}_{\text{aq,calc}} - \Delta G^{\text{reactants}}_{\text{aq,calc}} \quad \text{(S1)}$$

where $\Delta G^{\text{TS}}_{\text{aq,calc}}$ and $\Delta G^{\text{reactants}}_{\text{aq,calc}}$ are the quasithermodynamic quantity of the free energy of the transition state (TS) and the molar free energy of reactants, kcal/mol, respectively. The aqueous-phase free energy of activation at a given temperature is the sum of the standard state gaseous phase free energy of activation, $\Delta G^{\text{act}}_{\text{gas,calc}}$, and the solvation free energy of activation, $\Delta G^{\text{act}}_{\text{sol,calc}}$. Thus, following relationship can be written

$$\Delta G^{\text{act}}_{\text{aq,calc}} = \Delta G^{\text{act}}_{\text{gas,calc}} - \Delta G^{\text{act}}_{\text{solv,calc}} \quad \text{(S2)}$$

The use of an unrestricted DFT approach using the broken-symmetry (Guess=mix) method may result in the spin contamination, which affects the electronic energies of systems. Thus, we used an approximate spin-projection (AP) method.[9,10,11] According to the AP method, the spin-projected energy, E^{AP} atomic unit or kcal/mol, was calculated as

$$E^{\text{AP}} = \alpha E^{\text{BS}} - \beta E^{\text{HS}} \quad \text{(S3)}$$

where

$$\alpha = \frac{\langle S^2 \rangle^{\text{HS}}}{\langle S^2 \rangle^{\text{HS}} - \langle S^2 \rangle^{\text{BS}}}$$

$$\beta = \frac{\langle S^2 \rangle^{\text{BS}}}{\langle S^2 \rangle^{\text{HS}} - \langle S^2 \rangle^{\text{BS}}}$$

and E^{BS} is the energy of the broken symmetry at the singlet state, and E^{HS} is the energy of the high spin state such as triplet and quintet.

For the spin-projected Gibbs free energy, we added the thermal contribution to the spin-projected energy. We found five ‘unstable’ reactions and used the AP method to correct the energy and free energy values. Below includes the spin projected energies and free energies for each reaction.

$NO_2^{\bullet} + HO^{\bullet} \rightarrow ONOOH$

		E, au	Gcorr, au	<S2> before a	<S2> after ar	Projection coefficient		Projected Ene	EAP+ Gcorr
TS	singlet	-280.78817	-0.006881	0.9159	0.0464	1-a-b	0.55	-280.79288	-280.7998
	triplet	-280.78325		2.0084	2	a	0.45		
	quintet	-280.60953		6.0282	6.0003	b	0.00		

M06-2X/aug-cc-pvtz

	E, au (M06-2	ZPC (M06-2X,	Hcorr (M06-2	Gcorr, au (M06-2X/aug-cc-pvtz)	ΔG (kcal/mol)	
$NO_2^{\bullet}$ AQ	-205.0135			-0.014349		
$HO^{\bullet}$ AQ	-75.742068			-0.008573		
TS aq	-280.7929			-0.006881	-13.3	ΔG^{act}
					-23.4	ΔE^{act}

$NO_2^{\bullet} + HO^{\bullet} \rightarrow ONOOH$ (2 H_2O MOLECULES)

		E, au	Gcorr, au	<S2> before a	<S2> after ar	Projection coefficient		Projected Ene	EAP+ Gcorr
TS	singlet	-433.68644	0.034782	0.1497	0.0011	1-α-β	0.93	-433.6887	-433.65392
	triplet	-433.6586		2.0078	2	α	0.07		
	quintet	-433.43192		6.0001	6.0008	β	0.00		

M06-2X/aug-cc-pVTZ//M06-2X/cc-Pvdz 2H2O

	E, au (M06-2	ZPC (M06-2X	Hcorr (M06-2	Gcorr (M06-2	**ΔE (kcal/mol)**	**ΔE with ZPC (kcal/mol)**	**ΔH (kcal/mol)**	**ΔG (kcal/mol)**	
$NO_2^{\bullet}$ AQ	-205.01346			-0.018254					
$HO^{\bullet}$ AQ	-75.742013			-0.008573					
H2O	-76.44168			0.003491					
TS aq	-433.688701			0.034782				-1.8	ΔG^{act}

$NO_2^{\bullet} + NO_2^{\bullet} \rightarrow N_2O_4$

		E, au	Gcorr, au	<S2> before a	<S2> after ar	Projection coefficient		Projected Ene	EAP+ Gcorr
TS	singlet	-410.14099	-0.017328	1.0098	0.0789	1-α-β	0.50	-410.14251	-410.15983
	triplet	-410.14101		2.0103	2.0001	α	0.50		
	quintet	-409.90649		6.0223	6.0002	β	0.00		

	E, au CCSD(T	E, au (M06-2	ZPC (M06-2X	Hcorr (M06-2	Gcorr (M06-2	**ΔE (kcal/mol)**	**ΔE with ZPC (kcal/mol)**	**ΔH (kcal/mol)**	**ΔG (kcal/mol)**	
$NO_2^{\bullet}$ AQ	NA	-205.06958	0.008958	0.012827	-0.014357					
TS aq	NA	-410.142507	0.018524	0.026658	-0.017328					
									5.0	ΔG^{act}

$ONOO^- \rightarrow NO_3^-$

		E, au	Gcorr, au	<S2> before a	<S2> after ar	Projection coefficient		Projected Ene	EAP+ Gcorr
TS	singlet	-280.30704	-0.016159	0.9351	0.1603	1-a-b	0.55	-280.30409	-280.32025
	triplet	-280.31251		2.0549	2.0009	a	0.45		
	quintet	-280.18141		6.0258	6.0002	b	0.01		

	E, au (M06-2	ZPC (M06-2X	Hcorr (M06-2	E+Gcorr (M0	**ΔE (kcal/mol)**	**ΔE with ZPC (kcal/mol)**	**ΔH (kcal/mol)**	**ΔG (kcal/mol)**	
ONOO-				-280.39749					
TS aq				-280.32025					
								48.5	ΔG^{act}

$ONOOH \rightarrow NO_3^- + H^+$

		E, au	Gcorr, au	<S2> before a	<S2> after ar	Projection coefficient		Projected Ene	EAP+ Gcorr
	singlet	-357.23574	-0.005369	0.9109	0.0499	1-a-b	0.55	-357.2404	-357.24577
	triplet	-357.23087		2.009	2	a	0.45		
	quintet	-357.05605		6.0222	6.0002	b	0.00		

M06-2X/aug-cc-pVTZ//M06-2X/cc-Pvdz

	E, au (M06-2	ZPC (M06-2X	Hcorr (M06-2	Gcorr (M06-2	**ΔE (kcal/mol)**	**ΔE with ZPC (kcal/mol)**	**ΔH (kcal/mol)**	**ΔG (kcal/mol)**	
H2O	-76.44168			0.003491					
ONOOH	-280.84542			-0.002251					
TS aq	-357.240397			0.016477				38.9	ΔG^{act}

$NO_2^{\bullet} + O^{\bullet -} \rightarrow ONOO^-$

		E, au	Gcorr, au	<S2> before a	<S2> after ar	Projection coefficient		Projected Ene	EAP+ Gcorr
	singlet	-280.31354	-0.015798	0.8405	0.0509	1-a-b	0.58	-280.29771	-280.31351
	triplet	-280.33633		2.0147	2.0001	a	0.41		
	quintet	-280.22501		6.0228	6.0002	b	0.00		

M06-2X/aug-cc-pvtz

	E, au (M06-2	Gcorr (M06-2X/aug-cc-pvtz)	**ΔG (kcal/mol)**	
$NO_2^{\bullet}$ AQ	-205.0135	-0.014349		
$O^{\bullet -}$ AQ	-75.263314	-0.014569		
TS aq	-280.297710	-0.015798	-4.9	ΔG^{act}

We performed single point energy calculations using UCCSD(T)/cc-pVTZ (denoted as CCSDT) on the optimized structure obtained at the M05/Aug-cc-pVTZ (denoted as DFT) level. The aqueous phase free energy of activation for the single energy point calculation was obtained in the following manner:

$$\Delta G^{act}{}_{aq} = \Delta G^{act}{}_{gas} + [\Delta\Delta G^{act}{}_{solv}] \quad \text{(S4)}$$

where

$$\Delta G^{act}{}_{gas} = E(\mathrm{TS})_{\mathrm{CCSDT,gas}} + G_{\mathrm{corr}}(\mathrm{TS})_{\mathrm{DFT,gas}} - E(\mathrm{R1})_{\mathrm{CCSDT,gas}} - G_{\mathrm{corr}}(\mathrm{R1})_{\mathrm{DFT,gas}} - E(\mathrm{R2})_{\mathrm{CCSDT,gas}} - G_{\mathrm{corr}}(\mathrm{R2})_{\mathrm{DFT,gas}}$$

and

$$\Delta G^{act}{}_{gas} = \Delta E^{act}{}_{\mathrm{CCSDT,gas}} + \Delta G_{\mathrm{corr}}{}^{act}{}_{\mathrm{DFT,gas}}$$

$\Delta\Delta G^{act}{}_{solv}$ was calculated as

$$\Delta\Delta G^{act}{}_{solv} = \Delta G^{act}{}_{\mathrm{DFT,aq}} - \Delta G^{act}{}_{\mathrm{DFT,gas}}$$

$$\Delta\Delta G^{act}{}_{solv} = E(\mathrm{TS})_{\mathrm{DFT,aq}} + G_{\mathrm{corr}}(\mathrm{TS})_{\mathrm{DFT,aq}} - E(\mathrm{R1})_{\mathrm{DFT,aq}} - G_{\mathrm{corr}}(\mathrm{R1})_{\mathrm{DFT,aq}} - E(\mathrm{R2})_{\mathrm{DFT,aq}}$$

$$- G_{\mathrm{corr}}(\mathrm{R2})_{\mathrm{DFT,aq}} - (E(\mathrm{TS})_{\mathrm{DFT,gas}} + G_{\mathrm{corr}}(\mathrm{TS})_{\mathrm{DFT,gas}} - E(\mathrm{R1})_{\mathrm{DFT,gas}} - G_{\mathrm{corr}}(\mathrm{R1})_{\mathrm{DFT,gas}} - E(\mathrm{R2})_{\mathrm{DFT,gas}} - G_{\mathrm{corr}}(\mathrm{R2})_{\mathrm{DFT,gas}})$$

$$\Delta\Delta G^{act}{}_{solv} = \Delta E^{act}{}_{\mathrm{DFT,aq}} + \Delta G_{\mathrm{corr}}{}^{act}{}_{\mathrm{DFT,aq}} - \Delta E^{act}{}_{\mathrm{DFT,gas}} - \Delta G_{\mathrm{corr}}{}^{act}{}_{\mathrm{DFT,gas}}$$

Thus, we can write

$$\Delta G^{act}{}_{gas} + \Delta\Delta G^{act}{}_{solv} = \Delta E^{act}{}_{\mathrm{CCSDT,gas}} + \Delta G_{\mathrm{corr}}{}^{act}{}_{\mathrm{DFT,gas}} + \Delta E^{act}{}_{\mathrm{DFT,aq}} + \Delta G_{\mathrm{corr}}{}^{act}{}_{\mathrm{DFT,aq}} - \Delta E^{act}{}_{\mathrm{DFT,gas}} - \Delta G_{\mathrm{corr}}{}^{act}{}_{\mathrm{DFT,gas}}$$

$$\Delta G^{act}{}_{gas} + \Delta\Delta G^{act}{}_{solv} = \Delta E^{act}{}_{\mathrm{CCSDT,gas}} + \Delta E^{act}{}_{\mathrm{DFT,aq}} - \Delta E^{act}{}_{\mathrm{DFT,gas}} + \Delta G_{\mathrm{corr}}{}^{act}{}_{\mathrm{DFT,aq}}$$

where

$\Delta G^{act}{}_{gas}$ is the gaseous phase free energy of activation,

$\Delta\Delta G^{act}{}_{solv}$ is the free energy of solvation,

$E(\mathrm{TS})_{\mathrm{CCSDT,gas}}$ is the single point energy of TS calculated at the CCSDT/cc-pVTZ level in the gaseous phase,

$G_{\mathrm{corr}}(\mathrm{TS})_{\mathrm{DFT,gas}}$ is the thermal correction to the free energy of TS in the gaseous phase calculated with a DFT method (i.e. M05/Aug-cc-pVTZ),

$E(\mathrm{R1})_{\mathrm{CCSDT,gas}}$ and $E(\mathrm{R2})_{\mathrm{CCSDT,gas}}$ are the single point energies of reactants R1 and R2, respectively, at the CCSDT/cc-pVTZ level in the gaseous phase,

$G_{\mathrm{corr}}(\mathrm{R1})_{\mathrm{DFT,gas}}$ and $G_{\mathrm{corr}}(\mathrm{R2})_{\mathrm{DFT,gas}}$ are the thermal corrections to the free energy of the reactants R1 and R2, respectively, in the gaseous phase calculated with a DFT method,

$E(\mathrm{TS})_{\mathrm{DFT,aq}}$, $E(\mathrm{R1})_{\mathrm{DFT,aq}}$ and $E(\mathrm{R2})_{\mathrm{DFT,aq}}$ are the single point energies of TS and reactants R1 and R2, respectively, in the aqueous phase, calculated with a DFT method and the SMD solvation model,

$G_{\mathrm{corr}}(\mathrm{TS})_{\mathrm{DFT,aq}}$, $G_{\mathrm{corr}}(\mathrm{R1})_{\mathrm{DFT,aq}}$ and $G_{\mathrm{corr}}(\mathrm{R2})_{\mathrm{DFT,aq}}$ are the thermal corrections to the free energy of TS and reactants R1 and R2, respectively, in the aqueous phase calculated with a DFT method,

$E(\mathrm{TS})_{\mathrm{DFT,gas}}$, $E(\mathrm{R1})_{\mathrm{DFT,gas}}$ and $E(\mathrm{R2})_{\mathrm{DFT,gas}}$ are the single point energies of TS and reactants R1 and R2, respectively, in the gaseous phase calculated with a DFT method, and

$G_{corr}(TS)_{DFT,gas}$, $G_{corr}(R1)_{DFT,gas}$ and $G_{corr}(R2)_{DFT,gas}$ are the thermal corrections to the free energy of TS, and reactants R1 and R2, respectively, in the gaseous phase calculated with a DFT method. All units are in kcal/mol.

Text S2: Molecular oxygen addition to a carbon-centered radical

The ground state molecular oxygen ($^3O_2$) is known as a multi-reference system and may require a multireference method instead of a single-reference method. To investigate the degree of multireference state for our $^3O_2$ system, we obtained a T1 diagnostic value for three transition states for the $^3O_2$ addition reactions. The transition state geometries were obtained at the level of M06-2X/Aug-cc-pVTZ and we used the single point energy calculation at UCCSD(T)/cc-pVTZ for the T1 value employed in Molpro. We obtained 0.0296 and 0.0112 for doublet and quartet states of reaction 13 ($^{\bullet}CH_2NHCH_3 + O_2 \rightarrow {}^{\bullet}OOCH_2NHCH_3$), respectively, 0.0312 and 0.0115 for doublet and quartet states of reaction 39 $^{\bullet}CH(OH)_2 + O_2 \rightarrow {}^{\bullet}OOCH(OH)_2$), and 0.0290 and 0.0170 for doublet and quartet states of reaction 43 ($^{\bullet}COO^- + O_2 \rightarrow {}^{\bullet}OOCOO^-$). This analysis indicates that the transition states for these reactions implies insignificant multireference effects for reactions 13 and 43 and modest effect for reaction 39 (i.e., a T1 diagnostic of > 0.04 implies strong multireference effects and a value of > 0.03 implies some cause for concern).[12] As a comparison, we used UM05 DFT with the basis set of Aug-cc-pVTZ and UCCSD(T)/cc-pVTZ for the single point energy calculation based on the optimized structure obtained at UM05/Aug-cc-pVTZ. Table 1 includes the free energies of activation and reaction, and the activation energies for these three reactions. It turns out that we do not see significant differences in those energies. Based on the analyses of T1 diagnostic values and comparison to the other DFT and reliable CCSD(T) calculations, the use of a multireference method such as CASSCF or CASPT2 was not explored for these transition state.

Given that a ground-state molecular oxygen ($^3O_2$) is a triplet and a carbon-centered radical is a doublet, the spin of a transition state is a quartet by conserving the spin. The reaction product is a peroxyl radical and the spin is a doublet. In the process from the transition state to the product, a spin-flip occurs. Few studies appeared to account this spin-flip effect and correct the potential surface energies for the gaseous phase molecular oxygen addition and no studies reported this effect for the aqueous phase reaction. To reduce the uncertainty about the potential energy surface (note that it is not transition state) resulting from the doublet/quartet spin-flipping, Goldsmith et al. (2015)[13] developed a new method based on the doublet/quartet splitting to accurately calculate the gaseous-phase potential energy surface for R + O_2 system as a function of the C-O bond length. According to their method, the doublet/quartet splitting was computed using the same multireference method as for the doublet geometry optimization first. They then performed coupled-cluster calculations. According to their calculation results, insignificant different in the gaseous phase energy (<0.2-0.3 kcal/mol) was reported with and without the doublet/quartet splitting correction. As we obtained significantly larger free energies of activation for the quartet state, we only included the values obtained at the double state here.

Text S3: Marcus theory calculation for single electron transfer

Marcus theory[14,15] was originally developed to simulate the rate of electron transfer reactions in metal ions, and was later validated to calculate the free energy of activation for single electron transfer reactions in which organic molecules involved[16]. The theory uses two thermodynamic parameters: (1) standard free energy of reaction ($\Delta G^0_{\mathrm{SET}}$) and (2) reorganization energy (λ) to calculate the free energy of activation in equation S5 below.

$$\Delta G^{\mathrm{act}}_{\mathrm{SET}} = \frac{(\lambda + \Delta G^0_{\mathrm{SET}})^2}{4\lambda} \quad \text{(S5)}$$

$$\lambda = \lambda_{\mathrm{in}} + \lambda_{\mathrm{out}} \quad \text{(S6)}$$

$$\lambda_{\mathrm{in}} = \Delta E^0_{\mathrm{SET}} - \Delta G^0_{\mathrm{SET}} \quad \text{(S7)}$$

$$\Delta E^0_{\mathrm{SET}} = \Delta E^0_{\mathrm{vert\,product}} - \Delta E_{\mathrm{reactant}} \quad \text{(S8)}$$

where

$\Delta G^{\mathrm{act}}_{\mathrm{SET}}$ is the aqueous phase free energy of activation for single electron transfer, kcal/mol, $\Delta G^0_{\mathrm{SET}}$ is the aqueous phase free energy of reaction, kcal/mol, *l* is the reorganization energy, $\Delta E^0_{\mathrm{SET}}$ is the reaction energy change, $\Delta E^0_{\mathrm{vert\,product}}$ is the change in energy for vertical product and $\Delta E_{\mathrm{reactant}}$ is the energy of reactant. For this specific reaction, the term $\Delta G^0_{\mathrm{SET}}$ was calculated by obtaining the difference in the aqueous-phase free energy of formations between the sum of products (i.e., $NO_2^{\bullet}$ and OH^-) and the sum of reactants (NO_2^- and $HO^{\bullet}$). The reorganization term is the energy necessary to bring the structure of the reactants and surrounding solvent to those of the products[17]. The reorganization term is the energy necessary to bring the structure of the reactants and surrounding solvent to those of the products and has two components: (1) the inner shell, λ_{in}, that represents the change in the structure of solute and (2) the outer shell, λ_{out}, that represents the change in the structure of the surrounding solvent.[18]

λ_{out} was calculated according to the two-sphere model in a continuum medium was that proposed by Marcus

$$\lambda_{\mathrm{out}} = \Delta e^2 N_{\mathrm{A}} \left(\frac{1}{2r_1} + \frac{1}{2r_2} - \frac{1}{R} \right) \left(\frac{1}{\varepsilon_{\mathrm{o}}} - \frac{1}{\varepsilon_{\mathrm{s}}} \right) \quad \text{(S9)}$$

where

Δe is the amount of charge transferred,

N_{A} is Avogadro's number;

r_1 and r_2 are the ionic radii of the reactant molecules and $R = r_1 + r_2$.

ε_{o} and ε_{s} are the optic and static dielectric constants of water, with values of 78.39 and 1.77, respectively, at 25 °C.

The method to calculate the reorganization energy described above was verified by other studies[18-21]. The term $\Delta E^0_{\mathrm{SET}}$ was computed with single point energy calculations of

reactants and products. The term $\Delta E^{0}_{\text{vert product}}$ was computed with the energy of the optimized reactants with the charge and multiplicity obtained after the electron transfer occurs, and the term $\Delta E_{\text{reactant}}$ was computed as the energy of the reactants at the ground state. The difference between those two terms is called the non-adiabatic vertical energy, and is represented as a vertical transition between the reactant's and products's potential energy curves as shown in Figure S1 below.

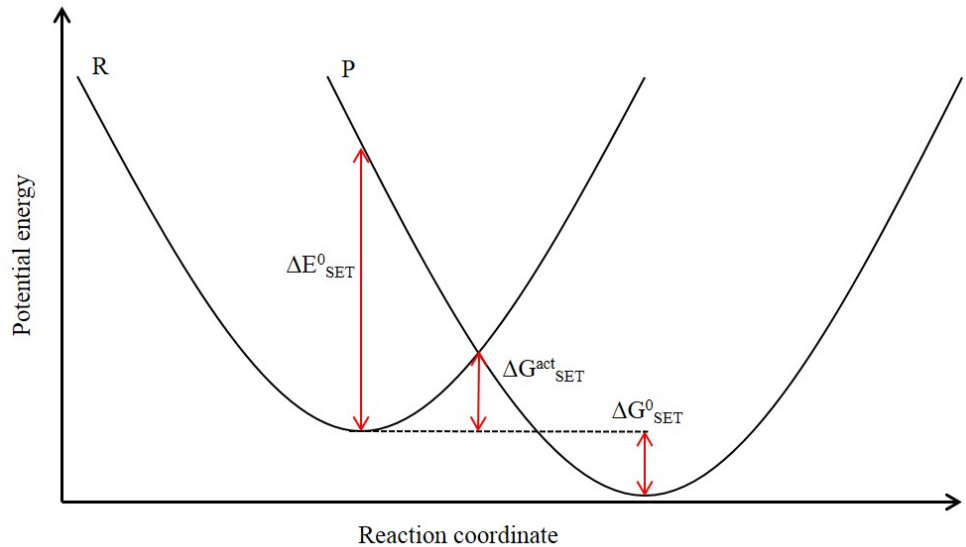

Figure S1: Each energy term defined in the potential energy surface of reactants (R) and products (P)

	Radius of a molecule, r, Å	G reactant, Hartrees	G product (SET), Hartrees	E reactant, Hartrees	Vertical energy, Hartrees	$\Delta E^{SET}_{calc,aq}$, kcal/mol (corrected)	$\Delta G^{rxn}_{calc,aq,SET}$, kcal/mol (corrected)	λ_o, kcal/mol	λ_i, kcal/mol	λ, kcal/mo	$\Delta G^{act}_{calc,aq,SET}$, kcal/mol (corrected)
$NO_2^{\bullet-}$	3.13	-205.282722	-205.083937	-205.26713	-205.04102	14.0	-2.7	16.6	2.5	19.1	3.5
$HO^{\bullet}$	2.3	-75.750508	-75.95353	-75.742068	-75.9458894						
r_o	1.77										
ε_s	78.39										
Δe	1										
Na	6.02E+23										

	Radius of a molecul	G reactant, H	G product (Sl	E reactant, H	Vertical energ	$\Delta E^{SET}_{calc,aq}$, kc	$\Delta G^{rxn}_{calc,aq,SET}$,	λSE_i, kcal/mol	λSEo, kcal/m	λSE, kcal/mo
$^{\bullet}CO_2^-$	3.15	-188.68857	-188.59965	-188.67366	-188.51651	81.9	0.0	81.9	2.170	84.035
CO_2	2.76	-188.59965	-188.68857	-188.58999	-188.61668					

	Radius of a molecul	G reactant, H	G product (Sl	E reactant, H	Vertical energ	$\Delta E^{SET}_{calc,aq}$, kc	$\Delta G^{rxn}_{calc,aq,SET}$,	λSE_i, kcal/mol	λSEo, kcal/m	λSE, kcal/mo
O_2	4.68	-150.34131	-150.4829	-150.32538	-150.44592	26.0	0.0	26.0	1.403	27.388
$^{\bullet}O_2^-$	4.4	-150.4829	-150.34131	-150.4661	-150.30415					

$^{\bullet}CO_2^- + O_2 \text{ --> } CO_2 + {}^{\square}O_2^-$	$\Delta G^{react}_{calc,aq,SET}$	λ, kcal/mol	$\Delta G^{act}_{calc,aq,SET}$, kcal/mol
	-33.1	55.7	2.3

Text S4: Experimental Apparatus and Procedure

According to Lee et al. (2005)[22], all experiments were performed in a 150 mL Pyrex reactor with a quartz material. The optical path length was 2 cm and a 13 W low-pressure mercury vapor lamp was used. The reaction solution was controlled at 25 ± 0.5 °C in a thermostatic water bath and the solution pH was adjusted by adding phosphate buffer and H_3PO_4. The measured incident photon intensity in this reactor was 1.87×10^{-6} einstein L^{-1}

s^{-1}. The photolysis experiments were initiated upon exposing the reactor to the UV irradiation.

Text S5: Sensitivity Analysis

Classic local sensitivity analysis was conducted to evaluate the importance of each reaction rate constant to the simulated time-dependent concentration profiles. We calculated the time-dependent sensitivity coefficient, $\left(\frac{k_j}{C_i}\frac{\partial C_i}{\partial k_j}\right)_t$ where k is the reaction rate constant of reaction j, Ci is the concentration of species i. The sensitivity coefficient was summered for all major species and each time point spanning the whole degradation process by calculating the overall sensitivity coefficient, $\sum_t \sum_i \left(\frac{k_j}{C_i}\frac{\partial C_i}{\partial k_j}\right)_t$. It is noted that a reaction rate constant with high overall sensitivity coefficient indicates that the reaction rate constant contributes to the overall concentration profile prediction significantly. Tables S1 and S2 show the sensitivity analysis results that rank the elementary reaction steps with the overall sensitivity coefficients at pH 3 and pH 7, respectively. At pH 3, the reactions related to NDMA initial transformation products (i.e., aminium radicals, *N*-methylidenmethylamine) showed the higher impact to the overall degradation of NDMA and the formation of methylamine and formaldehyde. At pH 7, in addition to those that relate to the initial NDMA transformation products, reactions involved in OONOOH/OONOO- and ONOOH/ONOO- showed significant contribution to the overall reactions. The ONOON/ONOO- react with HCHO to produce HCOOH/HCOO- or to produce nitrate via arrangement.

Table S1: Ranking of elementary reaction steps with overall sensitivity coefficients at pH 3

Pathway No.	Mechanisms	Elementary reaction	Overall sensitivity coefficient
8	Radical coupling	$(CH_3)_2{}^{\bullet}NH^+ + {}^{\bullet}NO \rightarrow CH_3N(+)H{=}CH_2 + HNO$	12.5
11	Hydrolysis	$CH_3N(+)H{=}CH_2 + H_2O \rightarrow CH_3NH_3{}^+ + HCHO$	11.0
33	H abstraction	$CH_2(OH)_2 + HO^{\bullet} \rightarrow {}^{\bullet}CH(OH)_2 + H_2O$	9.3
12	1,2-H shift	$(CH_3)_2{}^{\bullet}N \rightarrow {}^{\bullet}CH_2NHCH_3$	9.0
24	Isomerization	$ONOO^- \rightarrow NO_3{}^-$	7.2
38	H-abstraction	$HCOOH + HO^{\bullet} \rightarrow {}^{\bullet}COOH + H_2O$	6.9
39	H-abstraction	$HCOO^- + HO^{\bullet} \rightarrow {}^{\bullet}COO^- + H_2O$	6.9
16	Radical coupling	$NO^{\bullet} + HO^{\bullet} \rightarrow HNO_2$	6.6
31	Adduct formation	$HCHO + ONOO^- \rightarrow NO_2{}^- + HCOO^- + H^+$	6.5
13	O_2 addition	${}^{\bullet}CH_2NHCH_3 + O_2 \rightarrow {}^{\bullet}OOCH_2NHCH_3$	6.4
36	O2 addition	${}^{\bullet}CH(OH)_2 + O_2 \rightarrow {}^{\bullet}OOCH(OH)_2$	5.8
40	O2 addition	${}^{\bullet}COO^- + O_2 \rightarrow {}^{\bullet}OOCOO^-$	5.2
37	Unimolecular decay	${}^{\bullet}OOCH(OH)_2 \rightarrow HO_2{}^{\bullet} + HCOOH$	5.0
26	Radical coupling	$HO_2{}^{\bullet} + NO_2{}^{\bullet} \rightarrow OONOOH$	4.8
27	Radical coupling	$O_2{}^{\bullet-} + NO_2{}^{\bullet} \rightarrow OONOO^-$	4.8
30	Radical coupling and SET	$NO_2{}^- + HO^{\bullet} \rightarrow NO_2{}^{\bullet} + OH^-$	4.6
14	Radical coupling	$NO^{\bullet} + O_2{}^{\bullet-} \rightarrow ONOO^-$	3.8
15	Radical coupling	$NO^{\bullet} + HO_2{}^{\bullet} \rightarrow ONOOH$	3.8
41	Bimolecular decay	${}^{\bullet}OOCOO^- + {}^{\bullet}OOCOO^- \rightarrow 2{}^{\bullet}OCOO^-$	3.7
42	Alkoxyl radical decay	${}^{\bullet}OCOO^- + {}^{\bullet}OCOO^- \rightarrow O_2 + CO_2$	3.7
21	Radical coupling	$NO_2{}^{\bullet} + NO_2{}^{\bullet} \rightarrow N_2O_4$	3.3
34	H abstraction	$CH_2(OH)_2 + ONOO^- \rightarrow {}^{\bullet}CH(OH)_2 + H_2O$	2.6
35	H abstraction	$CH_2(OH)_2 + ONOOH \rightarrow {}^{\bullet}CH(OH)_2 + HNO2 +$	2.6
17	Radical coupling	$NO_2{}^{\bullet} + HO^{\bullet} \rightarrow ONOOH$	2.3
19	Radical coupling	$NO^{\bullet} + NO_2{}^{\bullet} \rightarrow N_2O_3$	1.0
23	Radical coupling	$NO^{\bullet} + NO^{\bullet} + (O_2) \rightarrow 2NO_2{}^{\bullet}$	1.0

Table S2: Ranking of elementary reaction steps with overall sensitivity coefficients at pH 7

Pathway No.	Mechanisms	Elementary reaction	Overall sensitivity coefficient
26	Radical coupling	$HO_2^{\bullet} + NO_2^{\bullet} \rightarrow OONOOH$	20.2
27	Radical coupling	$O_2^{\bullet -} + NO_2^{\bullet} \rightarrow OONOO^-$	20.2
14	Radical coupling	$NO^{\bullet} + O_2^{\bullet -} \rightarrow ONOO^-$	15
15	Radical coupling	$NO^{\bullet} + HO_2^{\bullet} \rightarrow ONOOH$	15
11	Hydrolysis	$CH_3N(+)H{=}CH_2 + H_2O \rightarrow CH_3NH_3^+ + HCHO$	13.3
12	1,2-H shift	$(CH_3)_2{}^{\bullet}N \rightarrow {}^{\bullet}CH_2NHCH_3$	11.5
8	Radical coupling	$(CH_3)_2{}^{\bullet}NH^+ + {}^{\bullet}NO \rightarrow CH_3N(+)H{=}CH_2 + HNO$	10.2
31	Adduct formation	$HCHO + ONOO^- \rightarrow NO_2^- + HCOO^- + H^+$	10.1
13	O_2 addition	${}^{\bullet}CH_2NHCH_3 + O_2 \rightarrow {}^{\bullet}OOCH_2NHCH_3$	8.2
24	Isomerization	$ONOO^- \rightarrow NO_3^-$	8
36	O2 addition	${}^{\bullet}CH(OH)_2 + O_2 \rightarrow {}^{\bullet}OOCH(OH)_2$	7.2
21	Radical coupling	$NO_2^{\bullet} + NO_2^{\bullet} \rightarrow N_2O_4$	5.7
33	H abstraction	$CH_2(OH)_2 + HO^{\bullet} \rightarrow {}^{\bullet}CH(OH)_2 + H_2O$	5
19	Radical coupling	$NO^{\bullet} + NO_2^{\bullet} \rightarrow N_2O_3$	4.8
23	Radical coupling	$NO^{\bullet} + NO^{\bullet} + (O_2) \rightarrow 2NO_2^{\bullet}$	4.8
17	Radical coupling	$NO_2^{\bullet} + HO^{\bullet} \rightarrow ONOOH$	2.1
37	Unimolecular decay	${}^{\bullet}OOCH(OH)_2 \rightarrow HO_2^{\bullet} + HCOOH$	1.9
34	H abstraction	$CH_2(OH)_2 + ONOO^- \rightarrow {}^{\bullet}CH(OH)_2 + H_2O$	1.2
35	H abstraction	$CH_2(OH)_2 + ONOOH \rightarrow {}^{\bullet}CH(OH)_2 + HNO2 +$	1.2
16	Radical coupling	$NO^{\bullet} + HO^{\bullet} \rightarrow HNO_2$	1.2
30	Radical coupling and SET	$NO_2^- + HO^{\bullet} \rightarrow NO_2^{\bullet} + OH^-$	0.93
38	H-abstraction	$HCOOH + HO^{\bullet} \rightarrow {}^{\bullet}COOH + H_2O$	0.84
39	H-abstraction	$HCOO^- + HO^{\bullet} \rightarrow {}^{\bullet}COO^- + H_2O$	0.84
40	O2 addition	${}^{\bullet}COO^- + O_2 \rightarrow {}^{\bullet}OOCOO^-$	0.19
42	Alkoxyl radical decay	${}^{\bullet}OCOO^- + {}^{\bullet}OCOO^- \rightarrow O_2 + CO_2$	0.16
41	Bimolecular decay	${}^{\bullet}OOCOO^- + {}^{\bullet}OOCOO^- \rightarrow 2{}^{\bullet}OCOO^-$	0.07

Text S6: Time-dependent DFT Analysis

TD-DFT calculations were performed at the level of M06-2X/Aug-cc-pVTZ with the SMD solvation method. We obtained two major and minor transitions at 202 nm and 347 nm and each canonical molecular orbital is shown in Figure S3. At 202 nm, we obtained HOMO-1→LUMO ($\pi \rightarrow \pi^*$ transition) (Figure S2) and HOMO→LUMO ($n \rightarrow \pi^*$) at 347 nm (Figure S3). The molecular orbitals (isovalue = 0.04) indicate that HOMO-1 is a π orbital delocalized over O-N-N of NDMA $(CH_3)_2NNO$, HOMO is a lone electron pair delocalized over O-N, and LUMO is a π orbital delocalized over O-N-N.

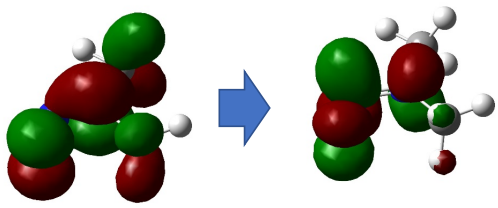

Figure S2: Molecular orbitals of HOMO-1 → LUMO

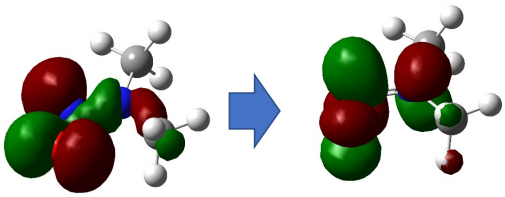

Figure S3: Molecular orbitals of HOMO → LUMO

Text S8: Thermodynamic property of 1,2-H shift of nitrogen-centered radical

This section explains how to determine a thermodynamic cycle for the 1,2-H shift reaction in the presence/absence of explicit solvent molecules.

$$\begin{array}{ccccc} R^{\bullet}_{(g)} & + & 2H_2O_{(g)} & \xrightarrow{\Delta G^{0,act} - 2\Delta G^{0\to *}} & TS_{(g)} \\ \Delta G^{*}_{solv}(R^{\bullet})\downarrow & & \Delta G^{*}_{solv}(H_2O)\downarrow & & \Delta G^{*}_{solv}(TS)\downarrow \\ R^{\bullet}_{(aq)} & + & 2H_2O_{(aq)} & \xrightarrow{\Delta G^{*,act} + 2RTLn(H_2O)} TS_{(aq)} & TS_{(aq)} \end{array}$$

where $\Delta G^{0,act}$ is the standard activation free energy in the gaseous phase, $\Delta G^{0\to *}$ is the correction accounting from the conversion of 1 mol of ideal gas at 1 atm to 1 M of ideal gas. This correction was carried out on every gaseous species, the ones for TS(g) and R(g) cancel out and 2 times $\Delta G^{0\to *}$ for the water molecules will remain. $\Delta G^{*}_{solv}(X)$ (X=R, TS and H_2O) is the solvation free energy of every species. The term 2RTLn([H_2O]) is the energy required to bring 2 moles of H_2O gas from 55.34 M liquid state to 1 M. Solving for $\Delta G^{*,act}$ yields

$$\begin{aligned} \Delta G^{0,act} &= TS_{(g)} - R^{\bullet}_{(g)} - 2H_2O_{(g)} + 2\Delta G^{0\to *} \\ \Delta G^{*,act} &= TS_{(aq)} - R^{\bullet}_{(aq)} - 2H_2O_{(aq)} - 2RTLn(55.34) \end{aligned} \qquad \text{(S11)}$$

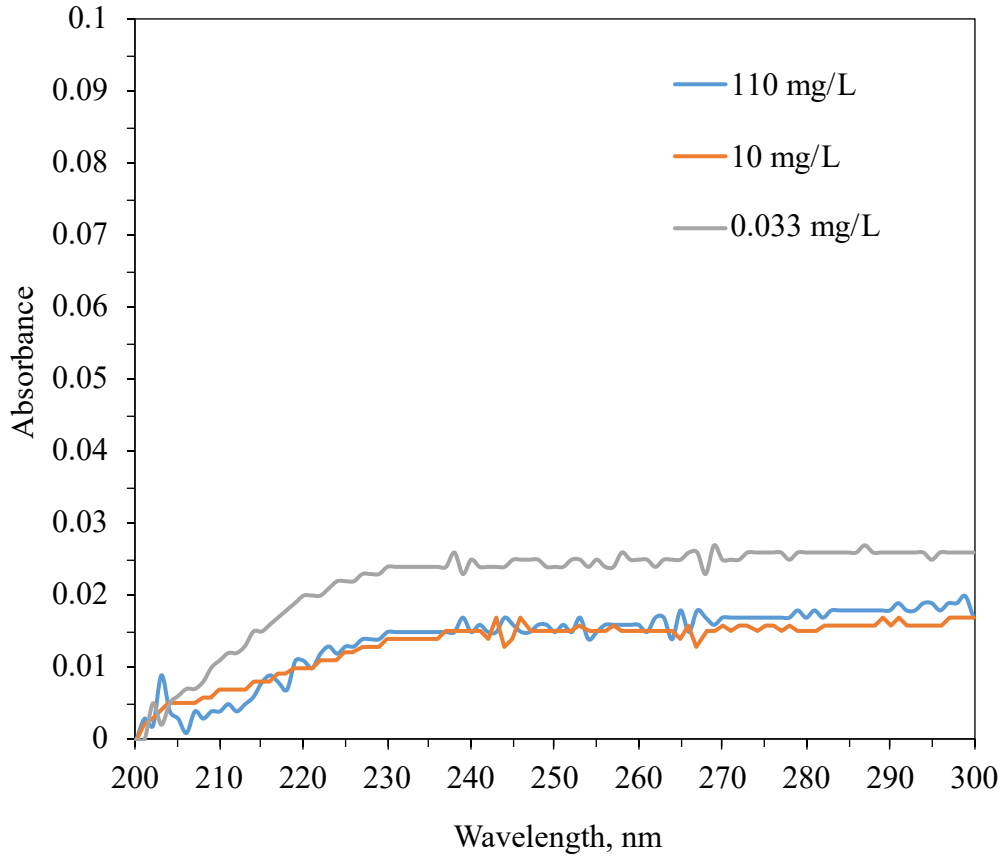

Figure S4: Absorbance of HCHO at around 254 nm of wavelength

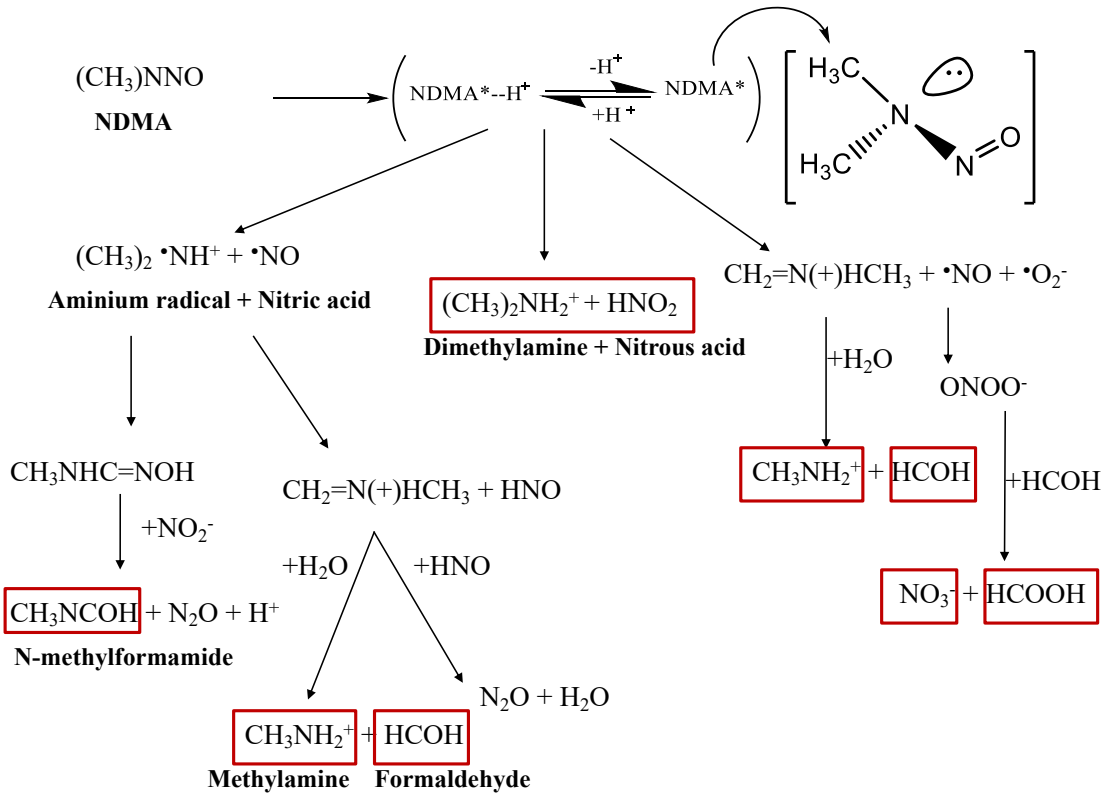

Figure S5: Experimentally proposed initial NDMA photochemical degradation pathways[22]

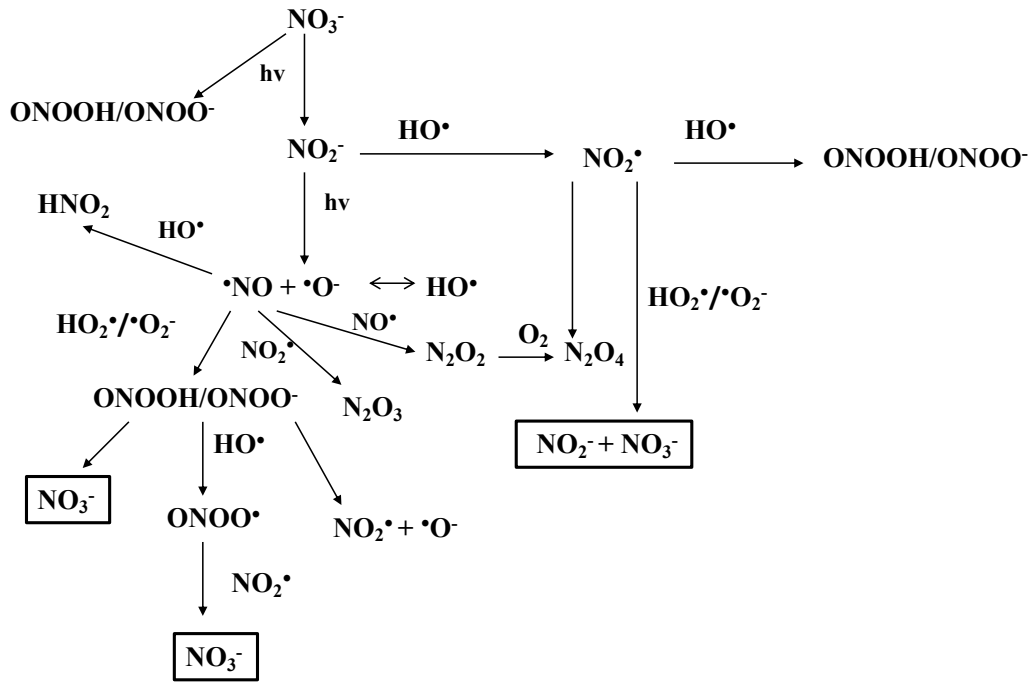

Figure S6: Experimentally proposed photochemical pathways of nitrate, nitrite, and peroxynitrous acid/peroxinitrite ions[25]

Text S9: Linear free energy relationship

If one aims to calculate the *k* value within a difference of a factor of 2 (i.e., typical experimental errors) from the experimental observation, the accuracy of ±0.4~0.5 kcal/mol of $\Delta G^{act}_{aq,calc}$ value would be required based on the conventiaonl trasition state theory ($k \propto \exp(-\Delta G^{act}_{aq,calc}/RT)$). Other researchers also argued that estimating of log *k* close to experimental accurage (~ 1 log (*k*)) would typically require an accuracy in $\Delta G^{act}_{aq,calc}$ value of < 2 kcal/ mol. Calculating the $\Delta G^{act}_{aq,calc}$ values within the errors described above, very high level method and basis set are required and the approach may be applicable only for small molecules. Thus, we determined the LFER between the $\Delta G^{act}_{aq,calc}$ values and the experimentally determined *k* values in the literature for the reactions of reactive nitrogen species undergoing radical-radical coupling to produce radical adducts (Figure S7). While many reactive nitrogen species react with other radical species at a rate close to the diffusion limit, the rate-determining step is the formation of a radical adduct in the cage. With a very limited number of data, the LFER is represented by $\ln k = -0.49\,\Delta G^{act}_{aq,calc} + 25.10$. In general, the M06-2X with a basis set of Aug-cc-pVTZ provides 0.3-1.3 kcal/mol average absolute deviation from the experimentally obtained gaseous-phase energy values.[78] The SMD solvation model provides mean unsigned errors of up to 1.0 kcal/mol in solvation free energies for neutral species and 4 kcal/mol on average for ionized species. Given that the estimated errors and the uncertainty resulting from the energies in the transition states are ±5.0 kcal/mol of $\Delta G^{act}_{aq,calc}$, all data points are within the range of 10 kcal/mol. We also estimated the range of ln*k* values are +0.42ln*k* and -0.49ln*k* with 95% confidence intervals. Thus, the LFER can be used to predict the rate constants for nitrogen-centered reactions whose rate constants have not been measured experimentally.

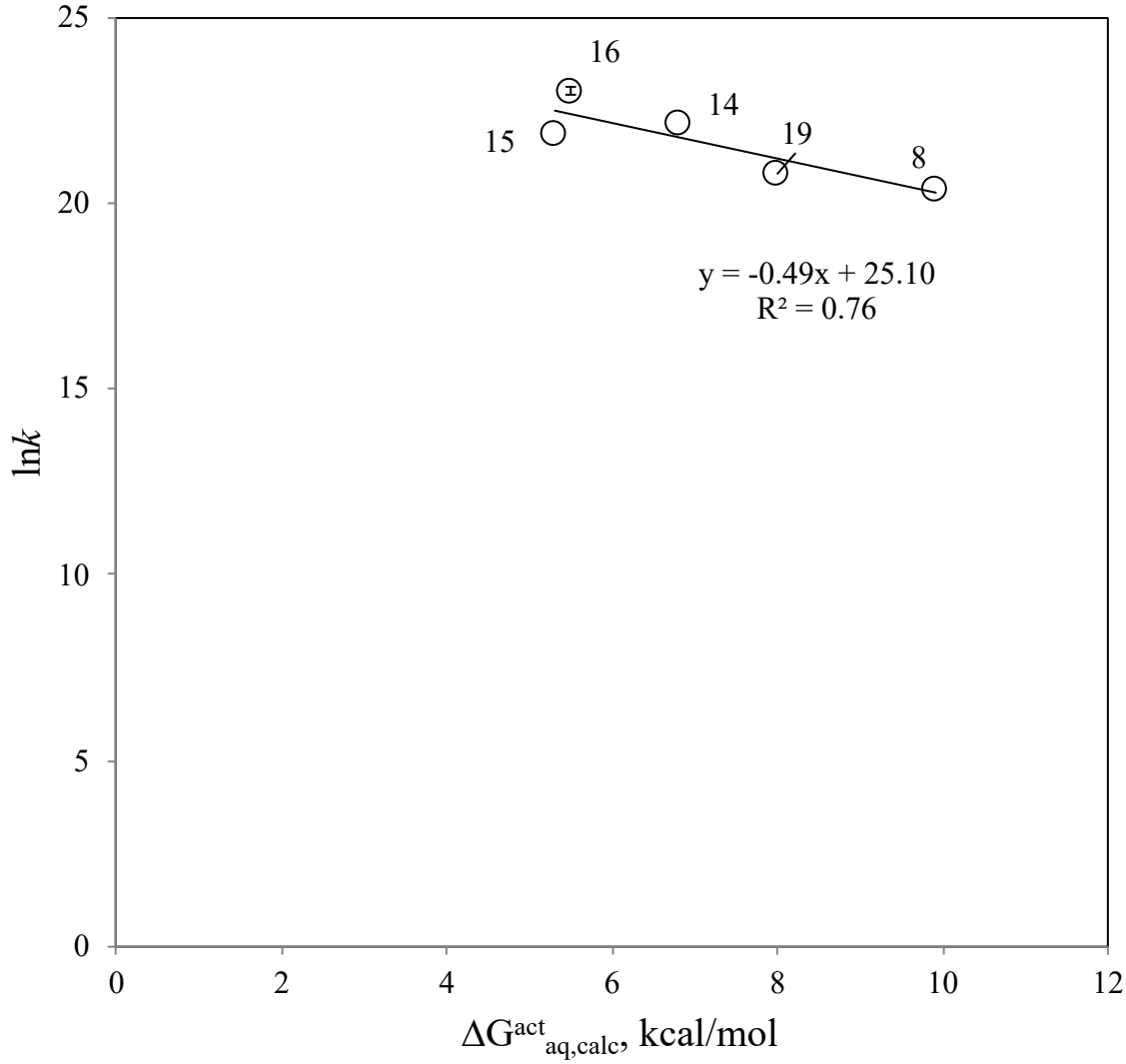

Figure S7: Linear free energy relationship between experimental *k* values and theoretically calculated aqueous-phase free energies of activation for reactive nitrogen species undergoing radical adduction formation. The vertical error bar represents the range of the experimental *k* values reported by various studies in the literature.

Literature Cited

1. H. B. Schlegel, Optimization of equilibrium geometries and transition structures *Journal of Computational Chemistry*, 1982, **3**, 214-218.
2. X. Li and M. J. Frisch, Energy-Represented Direct Inversion in the Iterative Subspace within a Hybrid Geometry Optimization Method *Journal of Chemical Theory and Computation*, 2006, **2**, 835-839.
3. C. Peng and H. Bernhard Schlegel, Combining Synchronous Transit and Quasi-Newton Methods to Find Transition States *Israel Journal of Chemistry*, 1993, **33**, 449-454.

4. C. Peng, P. Y. Ayala, H. B. Schlegel and M. J. Frisch, Using redundant internal coordinates to optimize equilibrium geometries and transition states *Journal of Computational Chemistry*, 1996, **17**, 49-56.
5. J. Pfaendtner and L. J. Broadbelt, Elucidation of structure–reactivity relationships in hindered phenols via quantum chemistry and transition state theory *Chemical Engineering Science*, 2007, **62**, 5232-5239.
6. E. Z. Wigner, f. physic. *Chemie,* 1932*,* **B19**, 203.
7. J. Pu, J. Gao and D. G. Truhlar, Multidimensional Tunneling, Recrossing, and the Transmission Coefficient for Enzymatic Reactions *Chemical Reviews*, 2006, **106**, 3140-3169.
8. M. D. Liptak and G. C. Shields, Accurate pKa Calculations for Carboxylic Acids Using Complete Basis Set and Gaussian-n Models Combined with CPCM Continuum Solvation Methods *Journal of the American Chemical Society*, 2001, **123**, 7314-7319.
9. T. Saito, S. Nishihara, Y. Kataoka, Y. Nakanishi, T. Matsui, Y. Kitagawa, T. Kawakami, M. Okumura and K. Yamaguchi, Transition state optimization based on approximate spin-projection (AP) method *Chemical Physics Letters*, 2009, **483**, 168-171.
10. T. Saito, S. Nishihara, Y. Kataoka, Y. Nakanishi, Y. Kitagawa, T. Kawakami, S. Yamanaka, M. Okumura and K. Yamaguchi, Reinvestigation of the Reaction of Ethylene and Singlet Oxygen by the Approximate Spin Projection Method. Comparison with Multireference Coupled-Cluster Calculations *The Journal of Physical Chemistry A*, 2010, **114**, 7967-7974.
11. B. Thapa, B. H. Munk, C. J. Burrows and H. B. Schlegel, Computational Study of Oxidation of Guanine by Singlet Oxygen (1Δg) and Formation of Guanine:Lysine Cross-Links *Chemistry – A European Journal*, 2017, **23**, 5804-5813.
12. T. J. Lee and P. R. Taylor, A diagnostic for determining the quality of single-reference electron correlation methods *International Journal of Quantum Chemistry*, 1989, **36**, 199-207.
13. C. F. Goldsmith, L. B. Harding, Y. Georgievskii, J. A. Miller and S. J. Klippenstein, Temperature and Pressure-Dependent Rate Coefficients for the Reaction of Vinyl Radical with Molecular Oxygen *The Journal of Physical Chemistry A*, 2015, **119**, 7766-7779.
14. R. A. Marcus, Chemical and Electrochemical Electron-Transfer Theory *Annual Review of Physical Chemistry*, 1964, **15**, 155-196.
15. R. A. Marcus, Electron transfer reactions in chemistry. Theory and experiment *Reviews of Modern Physics*, 1993, **65**, 599-610.
16. J. R. Miller, L. T. Calcaterra and G. L. Closs, Intramolecular long-distance electron transfer in radical anions. The effects of free energy and solvent on the reaction rates *Journal of the American Chemical Society*, 1984, **106**, 3047-3049.
17. T. P. Silverstein, Marcus Theory: Thermodynamics CAN Control the Kinetics of Electron Transfer Reactions *Journal of Chemical Education*, 2012, **89**, 1159-1167.
18. Y. Zhang, A. Moores, J. Liu and S. Ghoshal, New Insights into the Degradation Mechanism of Perfluorooctanoic Acid by Persulfate from Density Functional Theory and Experimental Data *Environmental Science & Technology*, 2019, **53**,

8672-8681.
19. S. F. Nelsen, S. C. Blackstock and Y. Kim, Estimation of inner shell Marcus terms for amino nitrogen compounds by molecular orbital calculations *Journal of the American Chemical Society*, 1987, **109**, 677-682.
20. C. Iuga, A. Campero and A. Vivier-Bunge, Antioxidant vs. prooxidant action of phenothiazine in a biological environment in the presence of hydroxyl and hydroperoxyl radicals: a quantum chemistry study *RSC Advances*, 2015, **5**, 14678-14689.
21. S. Luo, Z. Wei, D. D. Dionysiou, R. Spinney, W.-P. Hu, L. Chai, Z. Yang, T. Ye and R. Xiao, Mechanistic insight into reactivity of sulfate radical with aromatic contaminants through single-electron transfer pathway *Chemical Engineering Journal*, 2017, **327**, 1056-1065.
22. C. Lee, W. Choi and J. Yoon, UV Photolytic Mechanism of N-Nitrosodimethylamine in Water: Roles of Dissolved Oxygen and Solution pH *Environmental Science & Technology*, 2005, **39**, 9702-9709.
23. US EPA, 2017, ECOlogical Structure-Activity Relationship Model (ECOSAR) Class Program. V 2.0.
24. X. Guo, D. Minakata and J. Crittenden, Computer-Based First-Principles Kinetic Monte Carlo Simulation of Polyethylene Glycol Degradation in Aqueous Phase UV/H2O2 Advanced Oxidation Process *Environmental Science & Technology*, 2014, **48**, 10813-10820.
25. J. Mack and J. R. Bolton, Photochemistry of nitrite and nitrate in aqueous solution: a review *Journal of Photochemistry and Photobiology A: Chemistry*, 1999, **128**, 1-13.

Optimized transition states of each radical-involved reaction with z-matrix and intrinsic reaction coordinates

8 Radical coupling $(CH_3)_2{}^{\bullet}NH^+ + {}^{\bullet}NO \rightarrow CH_2{=}N^+HCH_3 + HNO$

TS:

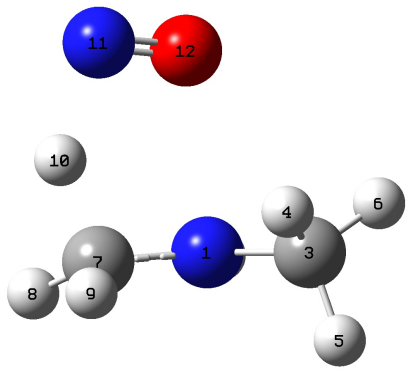

Row	Highlight	Display	Tag	Symbol	NA	NB	NC	Bond	Angle	Dihedral
1	No	Show	1	N						
2	No	Show	2	H	1			1.010023		
3	No	Show	3	C	1	2		1.453039	117.9724	
4	No	Show	4	H	3	1	2	1.088123	108.9362	155.1385
5	No	Show	5	H	3	1	2	1.090131	110.6472	-84.9269
6	No	Show	6	H	3	1	2	1.086266	109.354	35.5483
7	No	Show	7	C	1	3	6	1.345049	122.6613	-151.935
8	No	Show	8	H	7	1	3	1.084778	115.7621	-157.334
9	No	Show	9	H	7	1	3	1.086456	115.5734	-16.6805
10	No	Show	10	H	7	1	3	1.262769	107.2797	92.48301
11	No	Show	11	N	7	1	3	2.52987	84.85781	93.91702
12	No	Show	12	O	11	7	1	1.107233	85.82638	4.109751

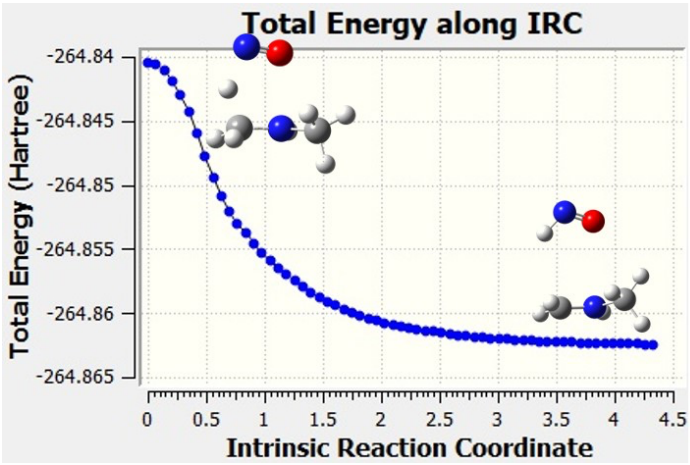

9 Dimerization 2HNO → HN(OH)-N=O

TS:

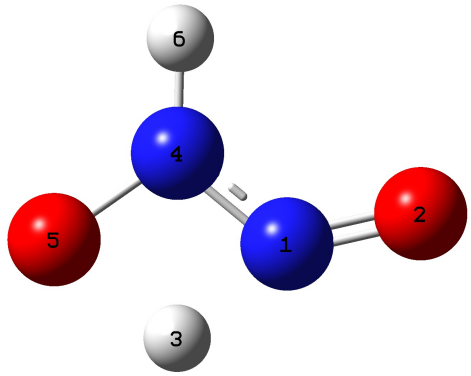

Row	Highlight	Display	Tag	Symbol	NA	NB	NC	Bond	Angle	Dihedral
1	No	Show	1	N						
2	No	Show	2	O	1			1.219279		
3	No	Show	3	H	1	2		1.287376	152.1062	
4	No	Show	4	N	1	2	3	1.264784	127.6465	-179.999
5	No	Show	5	O	4	1	2	1.340231	105.3886	179.9997
6	No	Show	6	H	4	1	2	1.022081	128.2086	-0.00215

IRC:

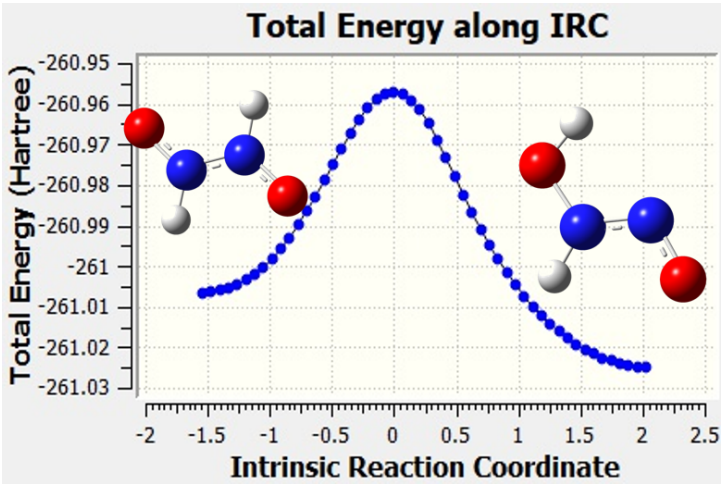

10 Arrangement HN(OH)-N=O → N_2O + H_2O

TS:

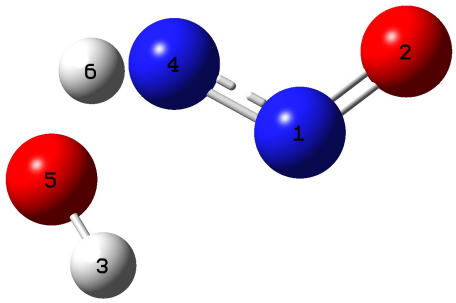

Row	Highlight	Display	Tag	Symbol	NA	NB	NC	Bond	Angle	Dihedral
1	No	Show	1	N						
2	No	Show	2	O	1			1.218232		
3	No	Show	3	H	1	2		2.209946	172.0196	
4	No	Show	4	N	1	2	3	1.310025	112.8216	77.60865
5	No	Show	5	O	4	1	2	1.560631	105.8201	-175.143
6	No	Show	6	H	4	1	2	1.217154	113.6369	-122.073

IRC:

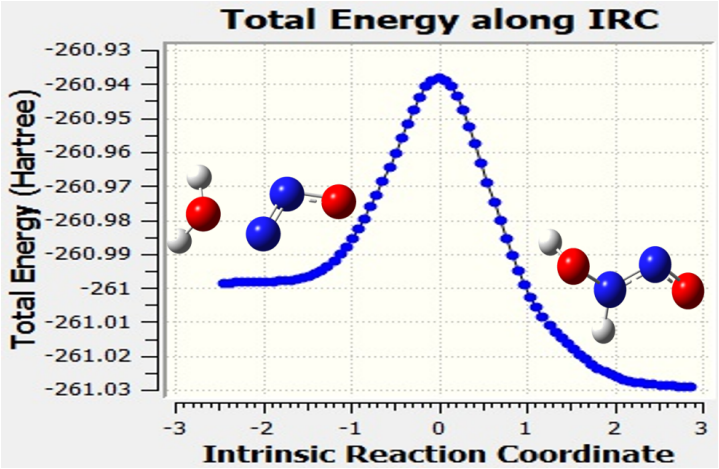

11 Hydrolysis $CH_2{=}N^+HCH_3 + H_2O \rightarrow CH_3NH_3^+ + HCHO$

TS:

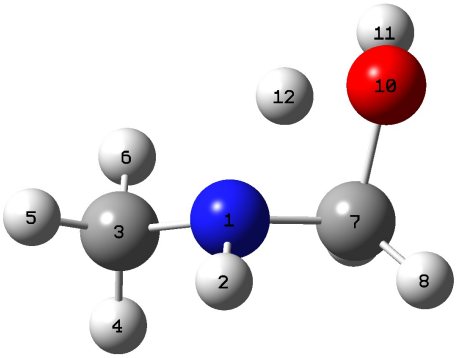

Row	Highlight	Display	Tag	Symbol	NA	NB	NC	Bond	Angle	Dihedral
1	No	Show	1	N						
2	No	Show	2	H	1			1.013817		

3	No	Show	3	C	1	2		1.470547	112.1048	
4	No	Show	4	H	3	1	2	1.088258	111.0502	-64.4188
5	No	Show	5	H	3	1	2	1.085693	108.7846	56.28705
6	No	Show	6	H	3	1	2	1.087606	108.6369	174.9791
7	No	Show	7	C	1	3	5	1.453111	115.5025	-173.211
8	No	Show	8	H	7	1	3	1.081855	113.4303	-136.302
9	No	Show	9	H	7	1	3	1.083644	114.3608	-4.12467
10	No	Show	10	O	7	1	3	1.475286	95.72383	111.1999
11	No	Show	11	H	10	7	1	0.972962	112.1773	-109.411
12	No	Show	12	H	10	7	1	1.172049	77.95121	0.850743

IRC:

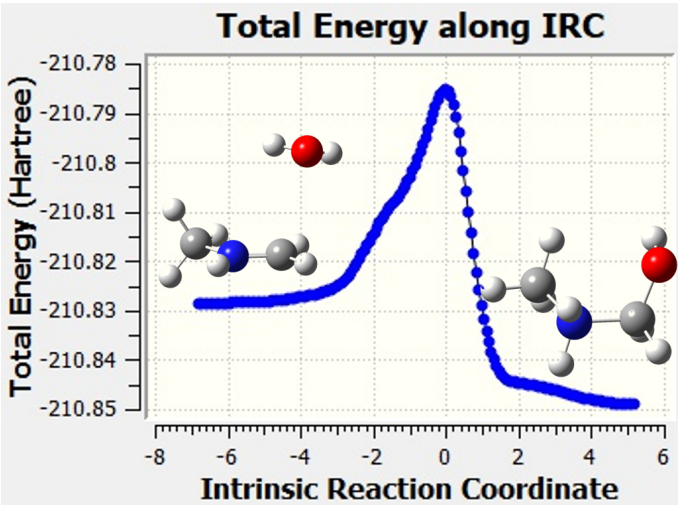

12 1,2-H shift $(CH_3)_2{}^{\bullet}N \rightarrow {}^{\bullet}CH_2NHCH_3$

TS:

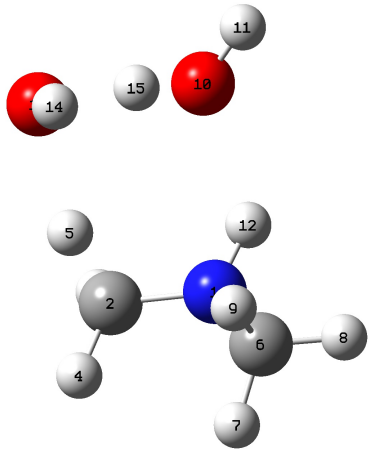

Row	Highlight	Display	Tag	Symbol	NA	NB	NC	Bond	Angle	Dihedral
1	No	Show	1	N						
2	No	Show	2	C	1			1.400548		

3	No	Show	3	H	2	1		1.091226	110.7186	
4	No	Show	4	H	2	1	3	1.084939	111.8787	127.1317
5	No	Show	5	H	2	1	3	1.147856	105.4604	-111.286
6	No	Show	6	C	1	2	4	1.432287	122.3179	-24.1141
7	No	Show	7	H	6	1	2	1.087189	109.5894	45.72969
8	No	Show	8	H	6	1	2	1.085143	109.8816	168.5776
9	No	Show	9	H	6	1	2	1.096601	108.5704	-72.4758
10	No	Show	10	O	1	2	6	2.789049	89.11949	-143.094
11	No	Show	11	H	10	1	2	0.961305	126.8692	150.1491
12	No	Show	12	H	1	2	6	1.026654	114.4175	-157.405
13	No	Show	13	O	10	1	2	2.527015	78.87972	43.64768
14	No	Show	14	H	13	10	1	0.961491	108.8023	75.2943
15	No	Show	15	H	10	1	2	1.039642	81.31272	46.37933

IRC:

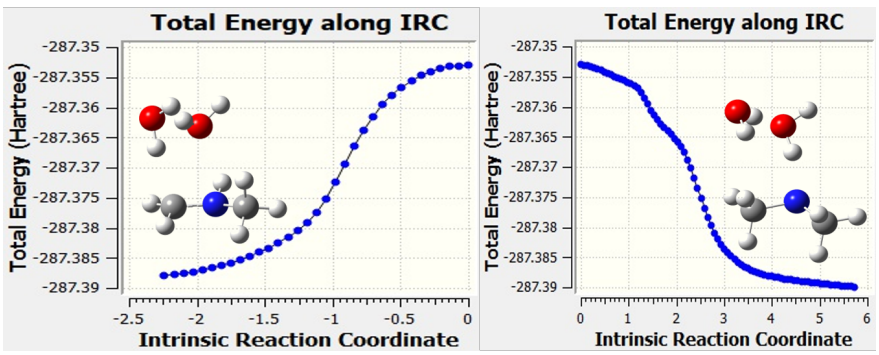

13 O_2 addition $^{\bullet}CH_2NHCH_3 + O_2 \rightarrow {}^{\bullet}OOCH_2NHCH_3$

TS:

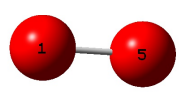

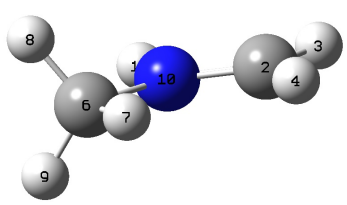

Row	Highlight	Display	Tag	Symbol	NA	NB	NC	Bond	Angle	Dihedral
1	No	Show	1	O						
2	No	Show	2	C	1			2.761061		
3	No	Show	3	H	2	1		1.080099	98.8727	
4	No	Show	4	H	2	1	3	1.080223	71.14386	120.2311
5	No	Show	5	O	1	2	3	1.318608	78.42065	-37.6717
6	No	Show	6	C	2	1	5	2.416771	91.1801	172.0169

7	No	Show	7	H	6	2	1	1.08473	83.23223	-71.4969
8	No	Show	8	H	6	2	1	1.086994	118.0624	38.20701
9	No	Show	9	H	6	2	1	1.086348	121.3566	178.2817
10	No	Show	10	N	2	1	5	1.268568	101.6273	-159.962
11	No	Show	11	H	10	2	1	1.017392	118.3531	105.6237

IRC:

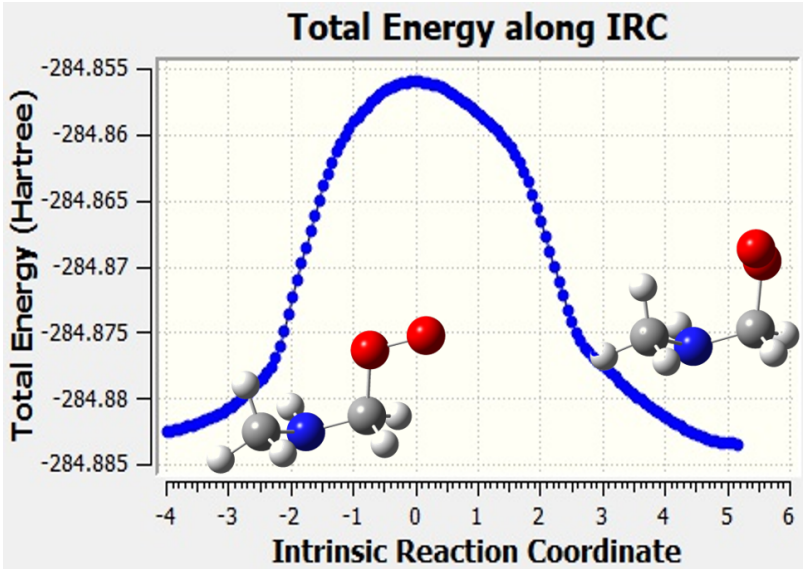

14 Radical coupling $NO^{\bullet} + O_2^{\bullet-} \rightarrow ONOO^-$

TS:

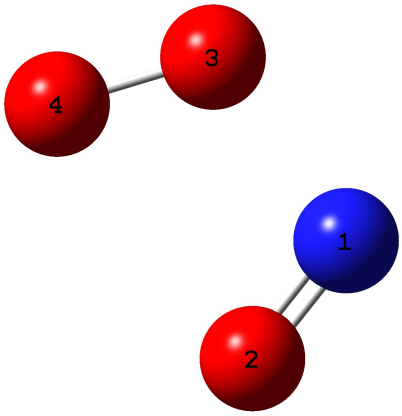

Row	Highlight	Display	Tag	Symbol	NA	NB	NC	Bond	Angle	Dihedral
1	No	Show	1	N						
2	No	Show	2	O	1			1.184751		
3	No	Show	3	O	1	2		1.78399	105.7419	
4	No	Show	4	O	3	1	2	1.279467	109.0697	0

IRC:

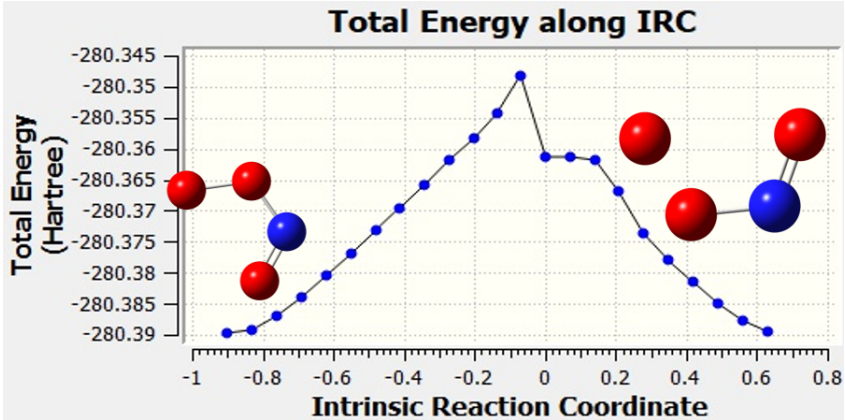

15 Radical coupling $NO^{\bullet} + HO_2^{\bullet} \rightarrow ONOOH$

TS:

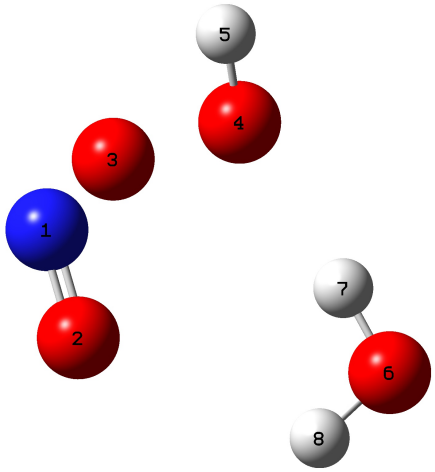

Row	Highlight	Display	Tag	Symbol	NA	NB	NC	Bond	Angle	Dihedral
1	No	Show	1	N						
2	No	Show	2	O	1			1.128744		
3	No	Show	3	O	1	2		1.587824	109.4596	
4	No	Show	4	O	3	1	2	1.404636	102.6829	-84.9792
5	No	Show	5	H	4	3	1	0.969619	104.037	-89.5105
6	No	Show	6	O	4	3	1	2.937419	105.5875	71.30595
7	No	Show	7	H	6	4	3	0.966492	3.856056	-143.329
8	No	Show	8	H	6	4	3	0.962426	102.4529	-21.4

IRC:

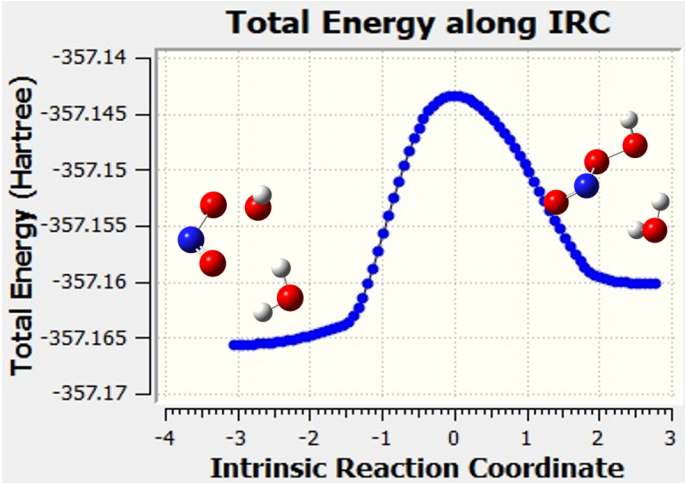

16 Radical coupling $NO^{\bullet} + HO^{\bullet} \rightarrow HNO_2$

TS:

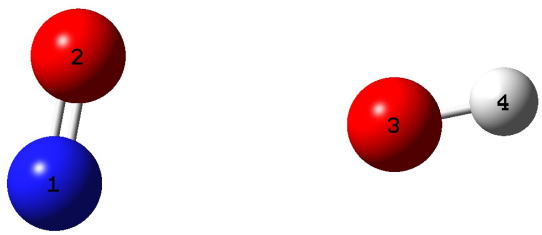

Row	Highlight	Display	Tag	Symbol	NA	NB	NC	Bond	Angle	Dihedral
1	No	Show	1	N						
2	No	Show	2	O	1			1.134253		
3	No	Show	3	O	2	1		2.82371	88.18454	
4	No	Show	4	H	3	2	1	0.974875	155.8732	-179.956

IRC:

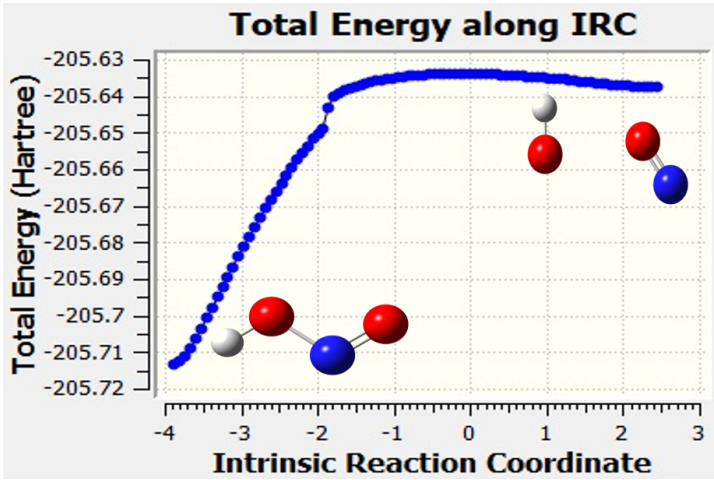

17 Radical coupling $NO_2^{\bullet} + HO^{\bullet} \rightarrow ONOOH$

TS:

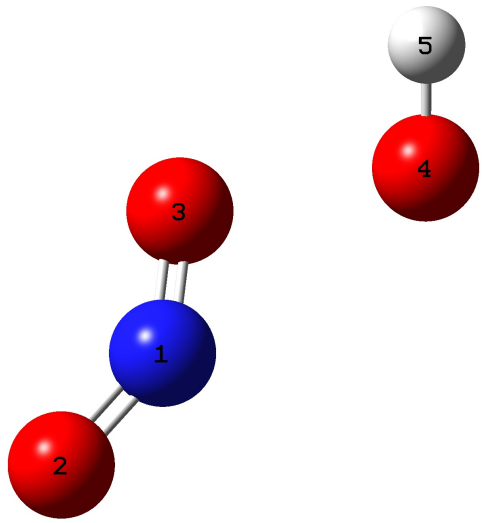

Row	Highlight	Display	Tag	Symbol	NA	NB	NC	Bond	Angle	Dihedral
1	No	Show	1	N						
2	No	Show	2	O	1			1.175115		
3	No	Show	3	O	1	2		1.140999	144.6084	
4	No	Show	4	O	3	1	2	1.935236	105.5969	-179.209
5	No	Show	5	H	4	3	1	0.967486	100.8164	-154.647

IRC:

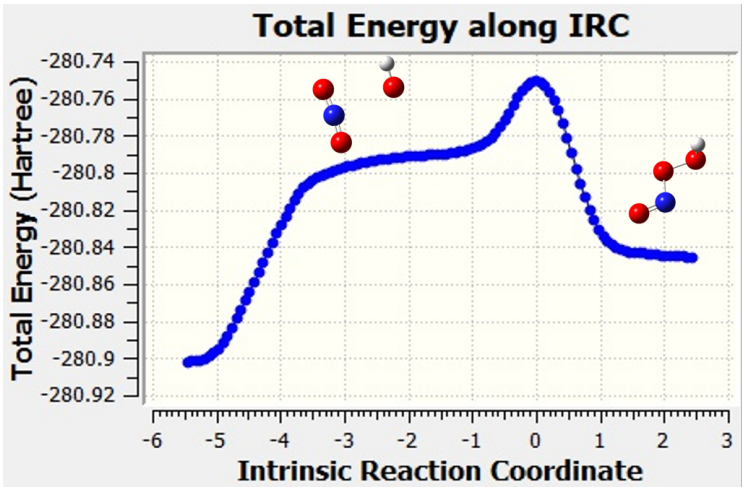

17_2H2O Radical coupling $NO_2^{\bullet} + O^{\bullet-} \rightarrow ONOOH$

TS:

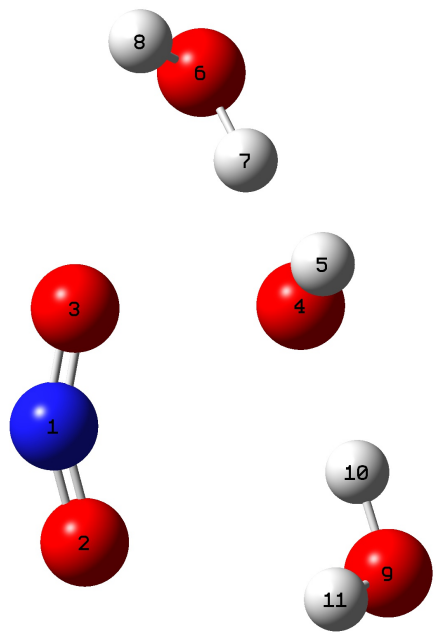

Row	Highlight	Display	Tag	Symbol	NA	NB	NC	Bond	Angle	Dihedral
1	No	Show	1	N						
2	No	Show	2	O	1			1.135871		
3	No	Show	3	O	1	2		1.12384	154.8411	
4	No	Show	4	O	3	1	2	2.140957	99.99734	1.064777
5	No	Show	5	H	4	3	1	0.971599	93.86887	-119.685
6	No	Show	6	O	4	3	1	2.643652	74.68597	143.0382
7	No	Show	7	H	6	4	3	0.997983	4.920063	-154.157
8	No	Show	8	H	6	4	3	0.967705	97.16565	45.81756
9	No	Show	9	O	4	3	1	2.651452	105.98	-15.6035
10	No	Show	10	H	9	4	3	0.999991	2.111311	132.7892
11	No	Show	11	H	9	4	3	0.967538	99.94072	-43.6759

IRC:

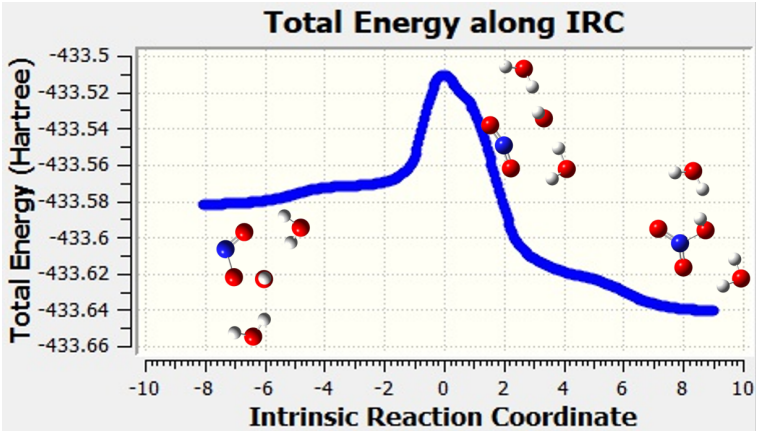

18 Radical coupling $NO_2^{\bullet} + O^{\bullet-} \rightarrow ONOO-$

TS:

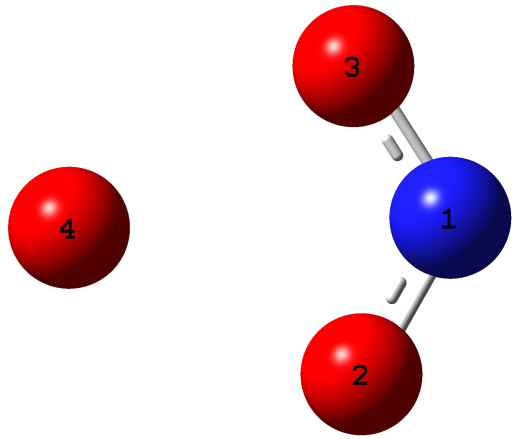

Row	Highlight	Display	Tag	Symbol	NA	NB	NC	Bond	Angle	Dihedral
1	No	Show	1	N						
2	No	Show	2	O	1			1.224662		
3	No	Show	3	O	1	2		1.224661	117.7718	
4	No	Show	4	O	2	1	3	2.227222	93.0307	0

IRC:

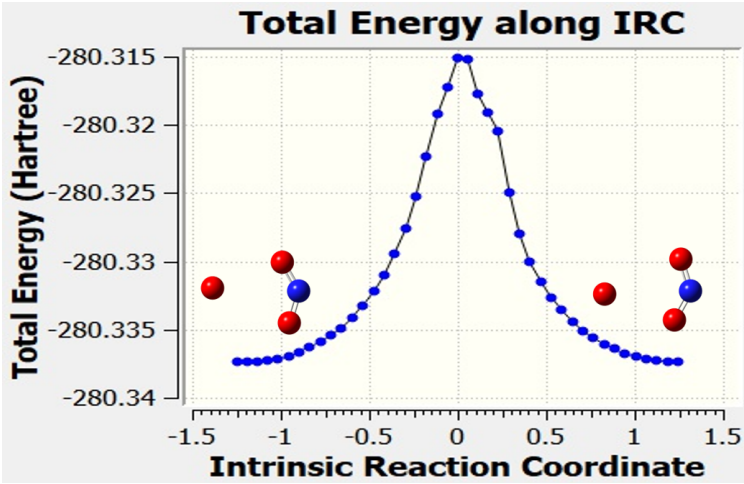

19 Radical coupling $NO^{\bullet} + NO_2^{\bullet} \rightarrow N_2O_3$

TS:

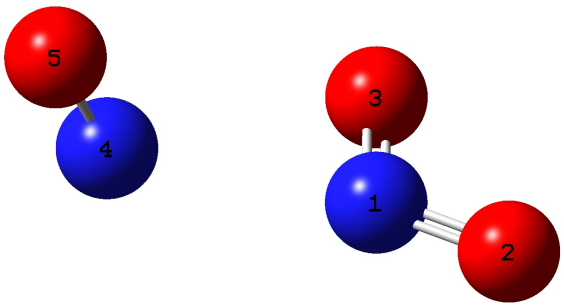

Row	Highlight	Display	Tag	Symbol	NA	NB	NC	Bond	Angle	Dihedral
1	No	Show	1	N						
2	No	Show	2	O	1			1.221179		

3	No	Show	3	O	1	2		1.244797	118.3855	
4	No	Show	4	N	1	2	3	2.258382	166.7044	-174.06
5	No	Show	5	O	4	1	2	1.063632	114.0459	80.37052

IRC:

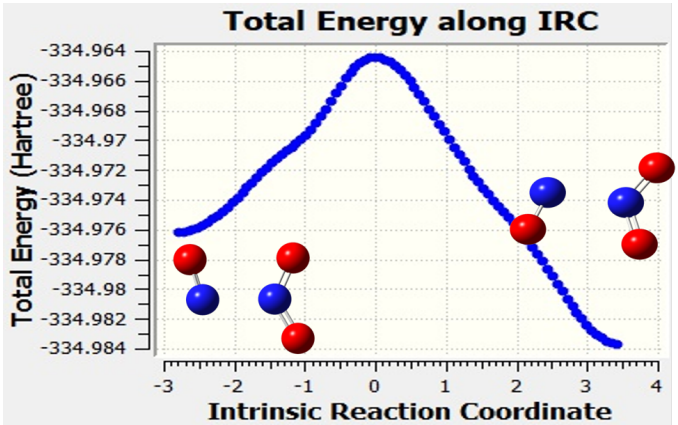

20 Radical coupling $NO_2^{\bullet} + NO_2^{\bullet} \rightarrow N_2O_4$

TS:

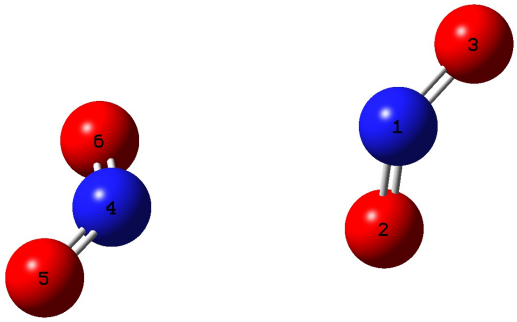

Row	Highlight	Display	Tag	Symbol	NA	NB	NC	Bond	Angle	Dihedral
1	No	Show	1	N						
2	No	Show	2	O	1			1.180353		
3	No	Show	3	O	1	2		1.179637	134.8457	
4	No	Show	4	N	2	1	3	3.142173	83.53608	-166.67
5	No	Show	5	O	4	2	1	1.179637	134.6524	-138.205
6	No	Show	6	O	4	2	1	1.180353	79.35859	76.4055

IRC:

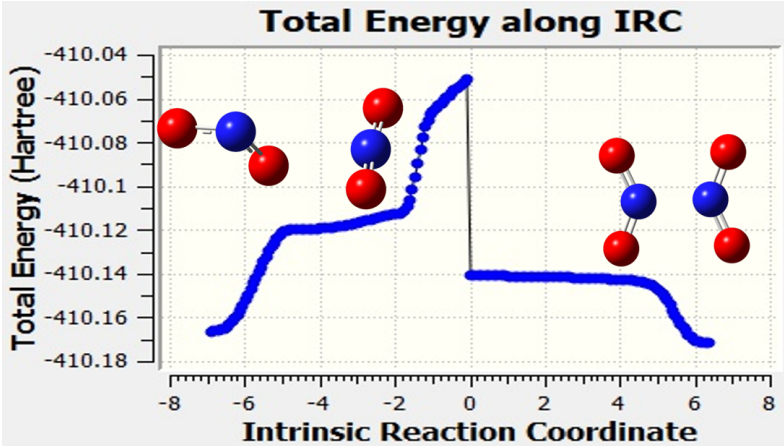

21 Radical coupling $NO^{\bullet} + NO^{\bullet} + (O_2) \rightarrow 2NO_2^{\bullet}$

TS:

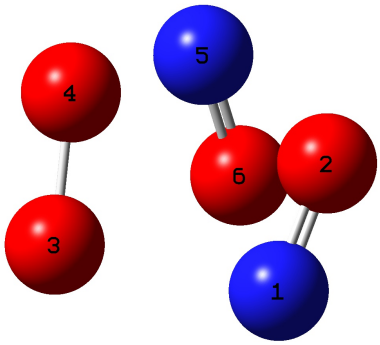

Row	Highlight	Display	Tag	Symbol	NA	NB	NC	Bond	Angle	Dihedral
1	No	Show	1	N						
2	No	Show	2	O	1			1.129084		
3	No	Show	3	O	1	2		2.289532	97.00527	
4	No	Show	4	O	3	1	2	1.268807	96.16076	-6.77903
5	No	Show	5	N	4	3	1	1.718525	106.5019	84.02138
6	No	Show	6	O	5	4	3	1.122813	106.7111	-1.07791

IRC:

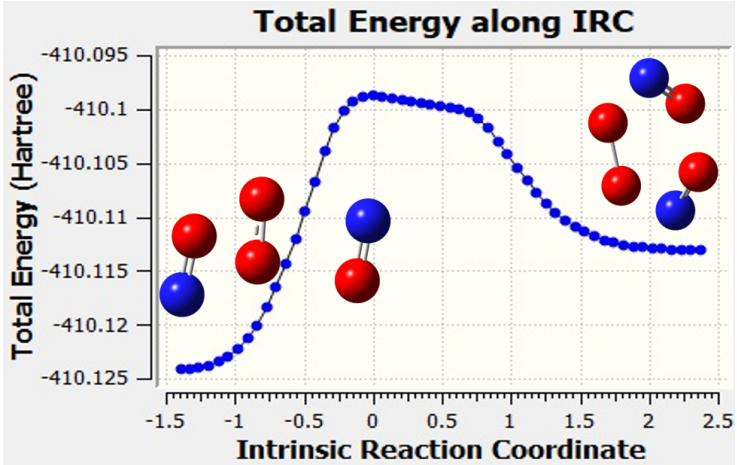

22 Isomerization $ONOO^- \rightarrow NO_3^-$

TS:

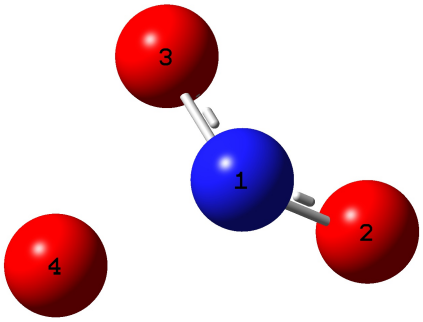

Row	Highlight	Display	Tag	Symbol	NA	NB	NC	Bond	Angle	Dihedral
1	No	Show	1	N						
2	No	Show	2	O	1			1.225855		
3	No	Show	3	O	1	2		1.268704	117.8504	
4	No	Show	4	O	1	2	3	1.710272	117.0021	89.80052

IRC:

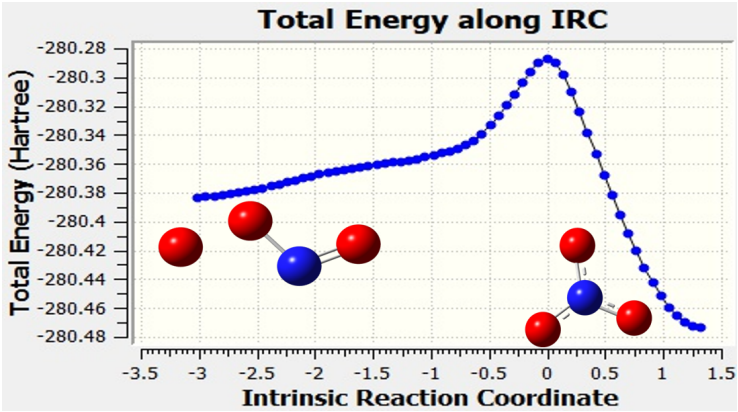

23 Isomerization $ONOOH \rightarrow NO_3^- + H^+$

TS:

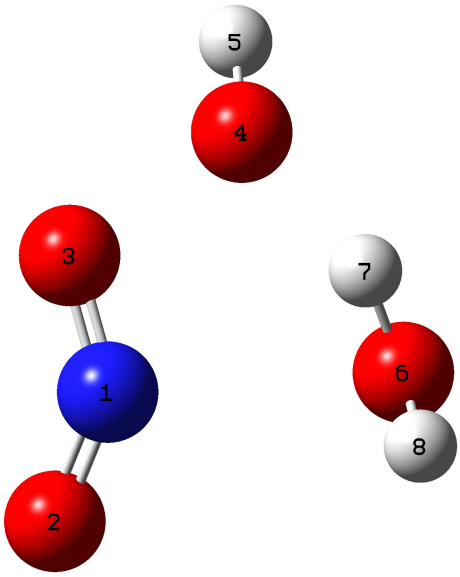

Row	Highlight	Display	Tag	Symbol	NA	NB	NC	Bond	Angle	Dihedral
1	No	Show	1	N						
2	No	Show	2	O	1			1.185506		
3	No	Show	3	O	1	2		1.161377	138.2938	
4	No	Show	4	O	3	1	2	1.935719	106.5204	178.7253
5	No	Show	5	H	4	3	1	0.97579	93.92725	142.2985
6	No	Show	6	O	1	3	4	2.441208	101.2914	-36.5907
7	No	Show	7	H	6	1	3	0.99222	72.0006	30.02515
8	No	Show	8	H	6	1	3	0.969272	90.38203	133.3529

IRC:

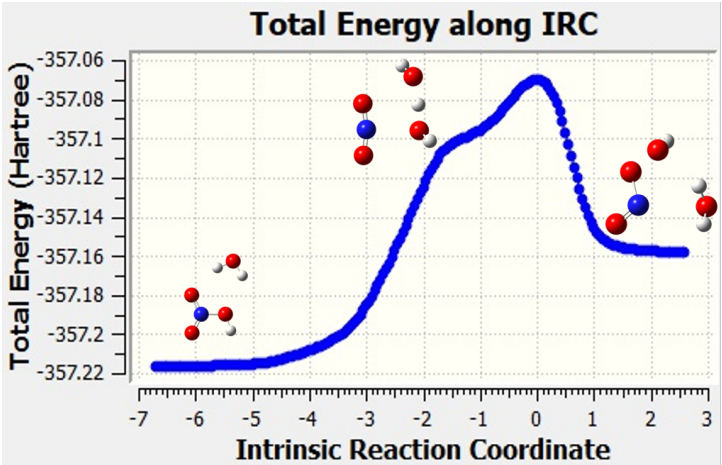

24 Radical coupling $HO_2^{\bullet} + NO_2^{\bullet} \rightarrow OONOOH$

TS:

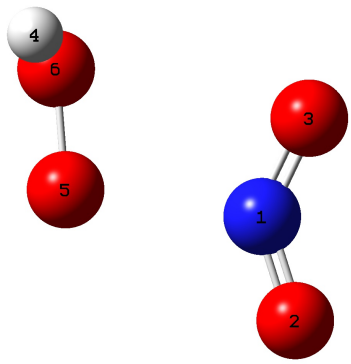

Row	Highlight	Display	Tag	Symbol	NA	NB	NC	Bond	Angle	Dihedral
1	No	Show	1	N						
2	No	Show	2	O	1			1.177158		
3	No	Show	3	O	1	2		1.176135	135.577	
4	No	Show	4	H	3	1	2	3.061606	81.70133	-164.003
5	No	Show	5	O	1	3	2	2.189447	108.6211	179.0126
6	No	Show	6	O	5	1	3	1.311818	103.4901	5.442259

IRC:

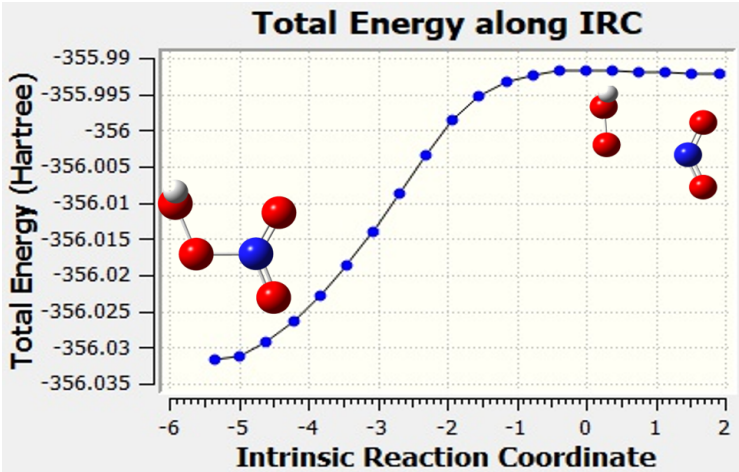

25 Radical coupling $O_2^{\bullet-} + NO_2^{\bullet} \rightarrow OONOO^-$

TS:

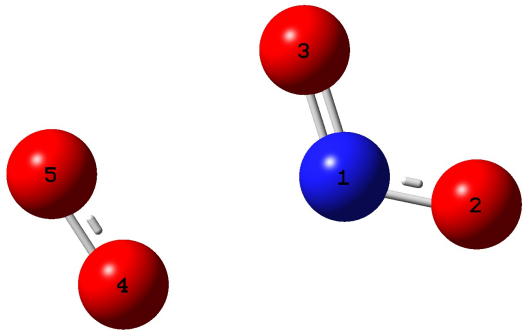

Row	Highlight	Display	Tag	Symbol	NA	NB	NC	Bond	Angle	Dihedral
1	No	Show	1	N						
2	No	Show	2	O	1			1.234329		
3	No	Show	3	O	1	2		1.223956	119.2426	
4	No	Show	4	O	1	3	2	2.254978	98.77267	179.9767
5	No	Show	5	O	4	1	3	1.211422	96.65757	0.147334

IRC:

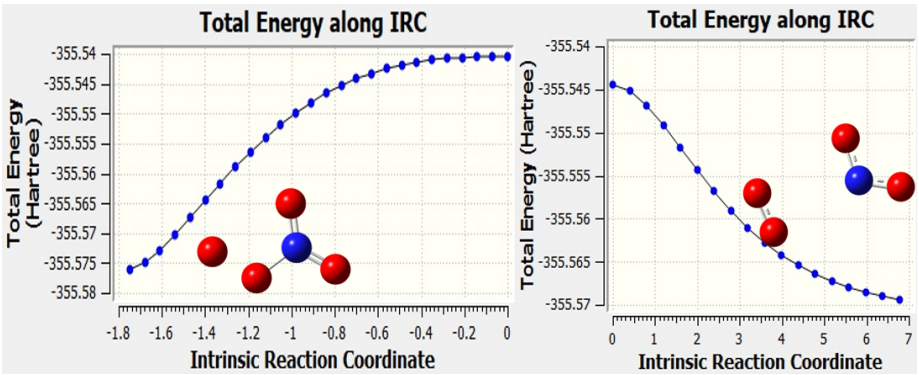

27 Adduct formation $HCHO + ONOO^- \rightarrow H_2C(ONOO\text{-})O$

TS:

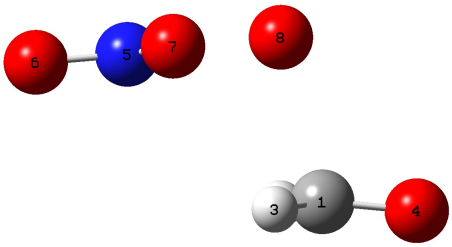

Row	Highlight	Display	Tag	Symbol	NA	NB	NC	Bond	Angle	Dihedral

1	No	Show	1	C						
2	No	Show	2	H	1			1.096537		
3	No	Show	3	H	1	2		1.096008	116.0614	
4	No	Show	4	O	1	3	2	1.223543	121.3407	-166.67
5	No	Show	5	N	1	4	2	3.297303	145.3456	-66.141
6	No	Show	6	O	5	1	4	1.190731	132.7175	-177.792
7	No	Show	7	O	5	1	4	1.332558	56.014	-89.6299
8	No	Show	8	O	7	5	1	1.40334	110.5155	51.66263

IRC:

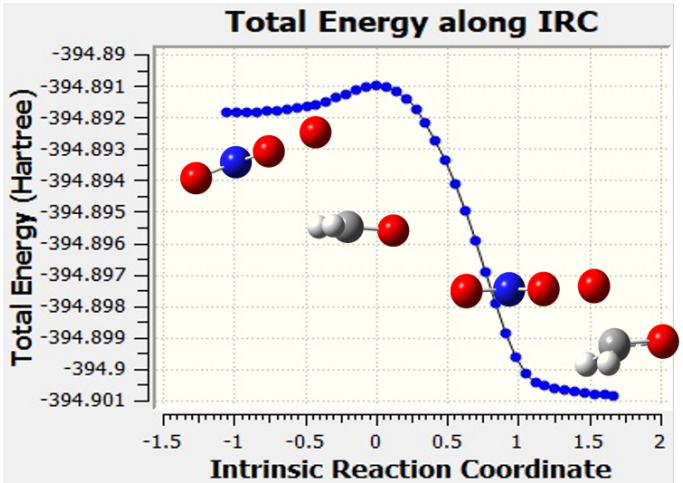

28 Hydrolysis $HCHO + H_2O \rightarrow CH_2(OH)_2$

TS:

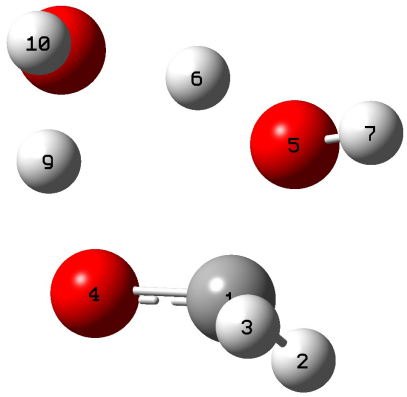

Row	Highlight	Display	Tag	Symbol	NA	NB	NC	Bond	Angle	Dihedral
1	No	Show	1	C						
2	No	Show	2	H	1			1.092503		
3	No	Show	3	H	1	2		1.096338	111.0263	
4	No	Show	4	O	1	2	3	1.328324	115.1757	-134.441
5	No	Show	5	O	1	4	2	1.561536	107.7813	113.6576
6	No	Show	6	H	5	1	4	1.131359	101.0369	35.73101
7	No	Show	7	H	5	1	4	0.968342	110.0583	152.36

8	No	Show	8	O	5	1	4	2.384374	89.21149	30.7187
9	No	Show	9	H	8	5	1	1.084392	72.04437	-16.1383
10	No	Show	10	H	8	5	1	0.964498	113.806	85.82181

IRC:

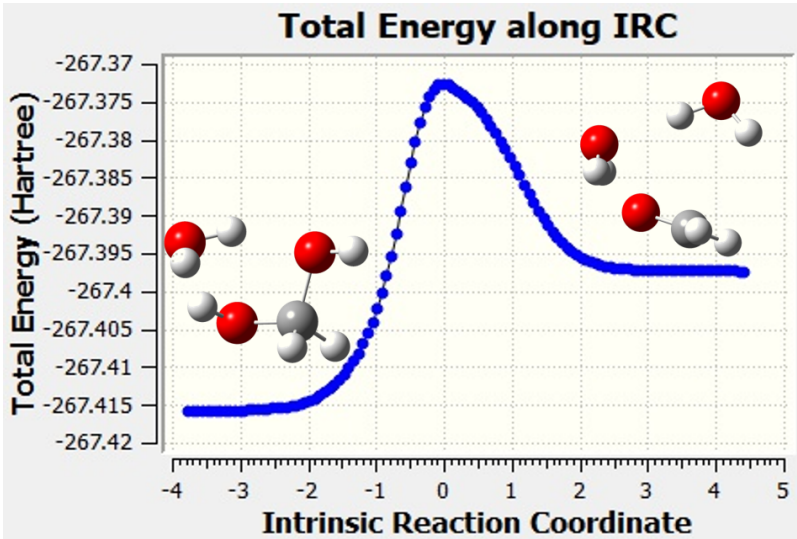

29 H abstraction $CH_2(OH)_2 + HO^{\bullet} \rightarrow {}^{\bullet}CH(OH)_2 + H_2O$

TS:

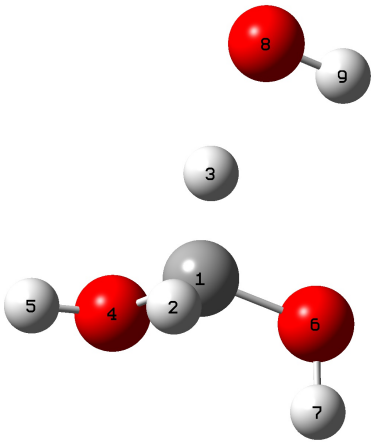

Row	Highlight	Display	Tag	Symbol	NA	NB	NC	Bond	Angle	Dihedral
1	No	Show	1	C						
2	No	Show	2	H	1			1.092308		
3	No	Show	3	H	1	2		1.139003	107.5303	
4	No	Show	4	O	1	2	3	1.399546	111.4568	-120.21
5	No	Show	5	H	4	1	2	0.96494	108.8074	35.92009
6	No	Show	6	O	1	4	5	1.390588	109.6394	161.5239
7	No	Show	7	H	6	1	4	0.965619	108.7834	-74.1727
8	No	Show	8	O	1	6	4	2.647095	94.13835	-114.889

9	No	Show	9	H	8	1	6	0.973489	85.64546	6.841973

IRC:

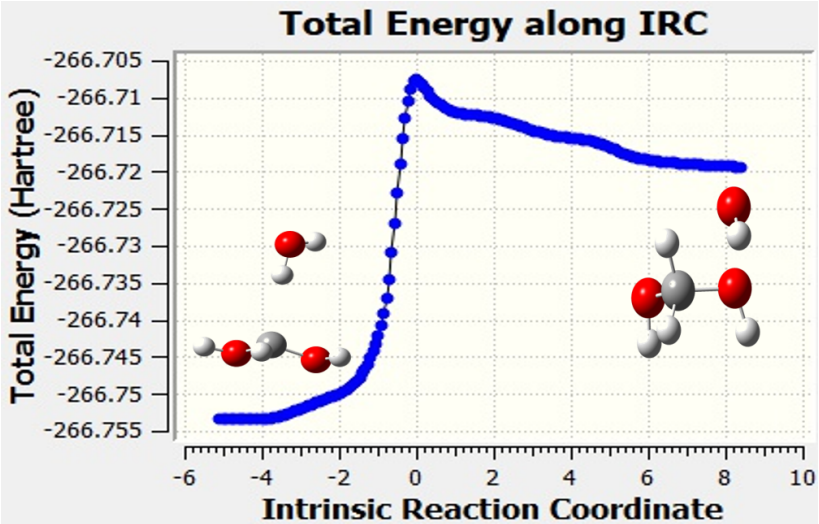

30 H abstraction $CH_2(OH)_2 + ONOO^- \rightarrow {}^{\bullet}CH(OH)_2 + NO_2^- + {}^{\square}OH$

TS:

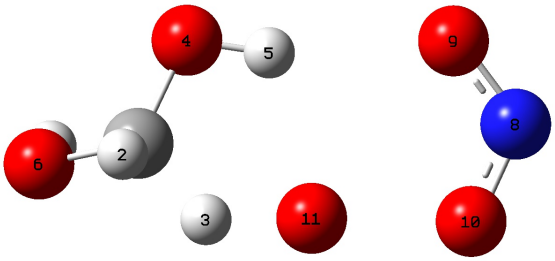

Row	Highlight	Display	Tag	Symbol	NA	NB	NC	Bond	Angle	Dihedral
1	No	Show	1	C						
2	No	Show	2	H	1			1.088422		
3	No	Show	3	H	1	2		1.225666	104.0836	
4	No	Show	4	O	1	2	3	1.38175	115.0732	-117.802
5	No	Show	5	H	4	1	2	0.975959	105.714	90.16909
6	No	Show	6	O	1	4	5	1.370457	112.0259	-144.133
7	No	Show	7	H	6	1	4	0.967834	108.8921	44.94105
8	No	Show	8	N	4	1	6	3.97744	101.3604	-138.556
9	No	Show	9	O	8	4	1	1.224088	38.98119	-157.766
10	No	Show	10	O	8	4	1	1.254582	79.50437	11.54389
11	No	Show	11	O	10	8	4	1.877537	113.7669	-2.85922

IRC:

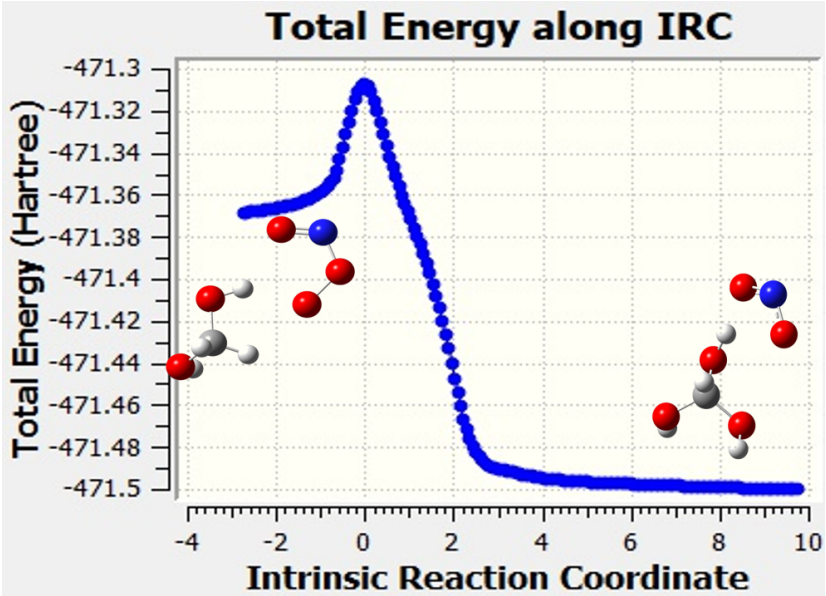

31 H abstraction $CH_2(OH)_2 + ONOOH \rightarrow {}^{\bullet}CH(OH)_2 + NO_2^{\bullet} + H_2O$

TS:

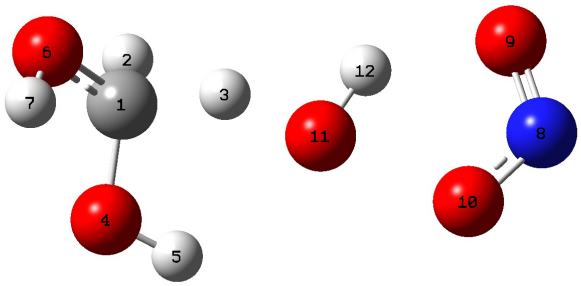

Row	Highlight	Display	Tag	Symbol	NA	NB	NC	Bond	Angle	Dihedral
1	No	Show	1	C						
2	No	Show	2	H	1			1.090827		
3	No	Show	3	H	1	2		1.291718	102.1041	
4	No	Show	4	O	1	2	3	1.358805	116.844	-111.721
5	No	Show	5	H	4	1	2	0.966231	109.2872	75.18959
6	No	Show	6	O	1	4	5	1.342352	112.6015	-154.631
7	No	Show	7	H	6	1	4	0.966202	108.9857	33.11591
8	No	Show	8	N	1	6	4	4.929653	128.6464	-115.604
9	No	Show	9	O	8	1	6	1.212494	67.43496	-79.6216
10	No	Show	10	O	8	1	6	1.23711	51.74025	93.66544
11	No	Show	11	O	10	8	1	1.902962	109.1024	-6.87873
12	No	Show	12	H	11	10	8	0.991566	82.70288	-0.59092

IRC:

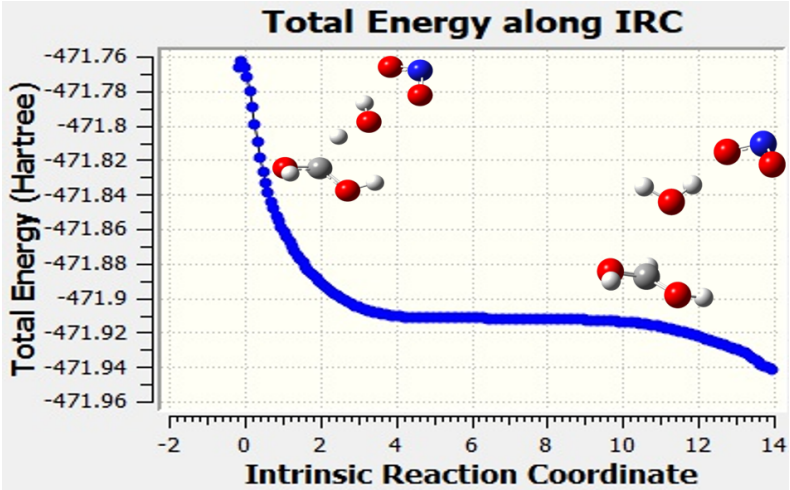

32 O_2 addition $^{\bullet}CH(OH)_2 + O_2 \rightarrow {}^{\bullet}OOCH(OH)_2$

TS:

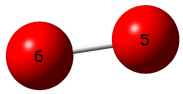

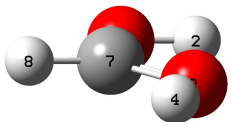

Row	Highlight	Display	Tag	Symbol	NA	NB	NC	Bond	Angle	Dihedral
1	No	Show	1	O						
2	No	Show	2	H	1			0.977622		
3	No	Show	3	O	1	2		2.192726	83.02645	
4	No	Show	4	H	3	1	2	0.974629	142.3286	178.0566
5	No	Show	5	O	3	1	2	3.00269	68.7049	102.4037
6	No	Show	6	O	5	3	1	1.318275	96.37117	66.98561
7	No	Show	7	C	1	3	5	1.263775	30.00688	-74.6506
8	No	Show	8	H	7	1	3	1.082047	117.6834	-177.387

IRC:

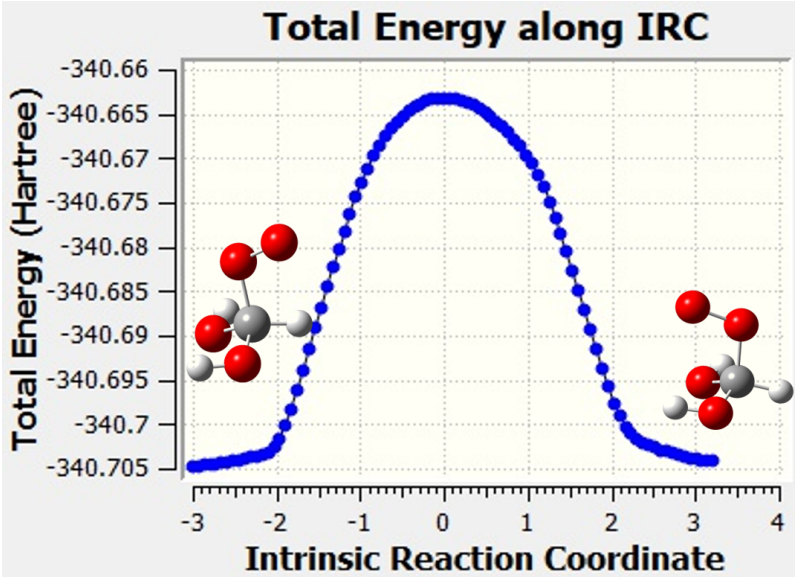

33 Unimolecular decay $^{\bullet}OOCH(OH)_2 \rightarrow HO_2^{\bullet} + HCOOH$

TS:

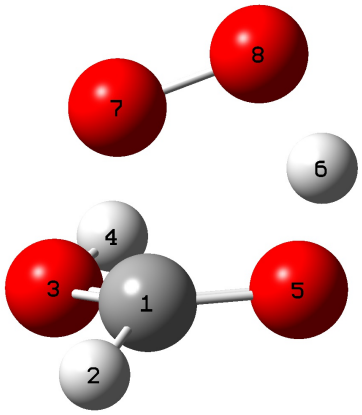

Row	Highlight	Display	Tag	Symbol	NA	NB	NC	Bond	Angle	Dihedral
1	No	Show	1	C						
2	No	Show	2	H	1			1.085515		
3	No	Show	3	O	1	2		1.326388	112.5593	
4	No	Show	4	H	3	1	2	0.971201	109.6256	-171.803
5	No	Show	5	O	1	3	4	1.280122	120.4344	-17.5538
6	No	Show	6	H	5	1	3	1.176965	101.3776	109.9622
7	No	Show	7	O	1	5	3	1.904522	95.99728	-109.185
8	No	Show	8	O	7	1	5	1.277093	102.1399	-0.09817

IRC:

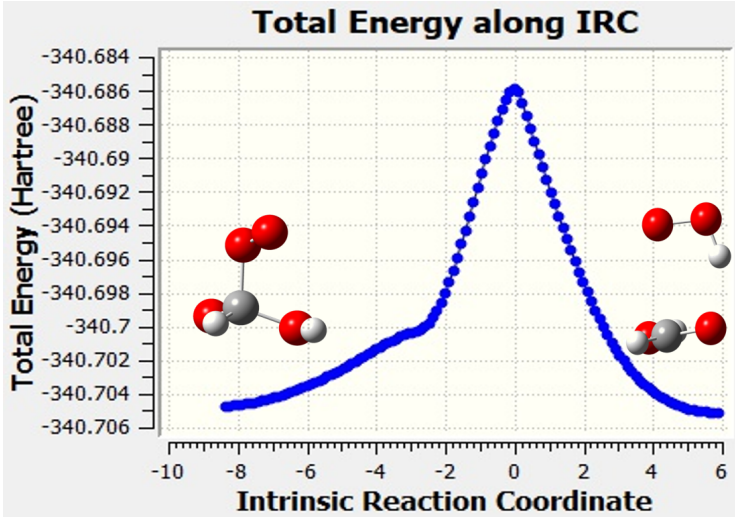

34 H-abstraction $HCOOH + HO^{\bullet} \rightarrow {}^{\bullet}COOH + H_2O$

TS:

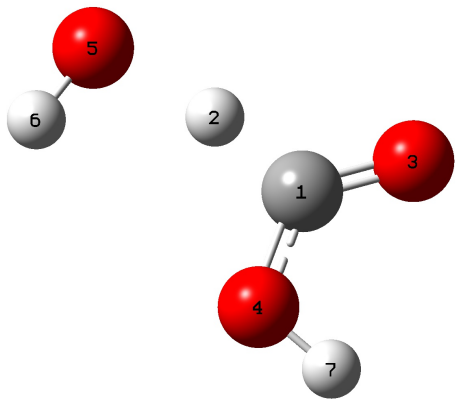

Row	Highlight	Display	Tag	Symbol	NA	NB	NC	Bond	Angle	Dihedral
1	No	Show	1	C						
2	No	Show	2	H	1			1.168489		
3	No	Show	3	O	1	2		1.194961	122.4028	
4	No	Show	4	O	1	3	2	1.318482	127.4874	179.9969
5	No	Show	5	O	1	3	4	2.577986	128.581	-179.961
6	No	Show	6	H	5	1	3	0.974074	92.94624	179.8887
7	No	Show	7	H	4	1	3	0.974528	110.1215	-0.01173

IRC:

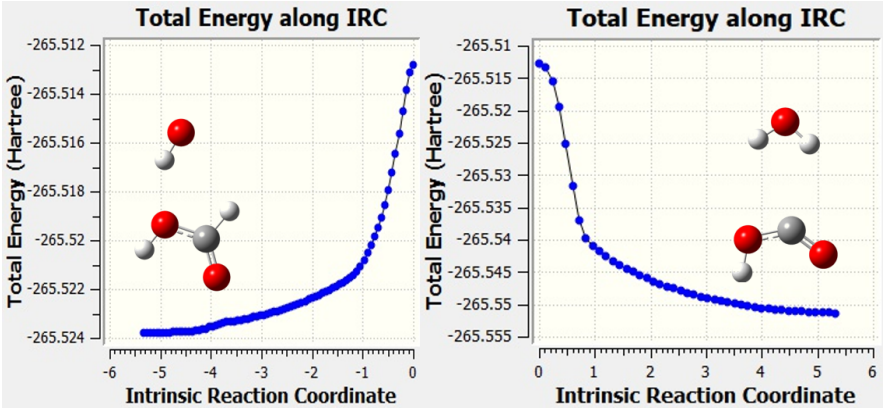

35 H-abstraction $HCOO^- + HO^\bullet \rightarrow {}^\bullet COO^- + H_2O$

TS:

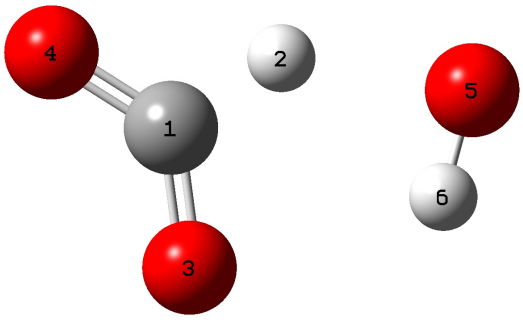

Row	Highlight	Display	Tag	Symbol	NA	NB	NC	Bond	Angle	Dihedral
1	No	Show	1	C						
2	No	Show	2	H	1			1.14762		
3	No	Show	3	O	1	2		1.244288	114.8475	
4	No	Show	4	O	1	3	2	1.241922	129.8978	180
5	No	Show	5	O	1	4	3	2.665931	140.4793	179.9937
6	No	Show	6	H	5	1	4	0.97446	67.7975	-179.992

IRC: